Controllable-pitch propeller design process for a wind-powered car-carrier optimising for total energy consumption

Ocean Engineering 269 (2023) 113426

Contents lists available at ScienceDirect

Ocean Engineering

journal homepage: www.elsevier.com/locate/oceaneng

Controllable-pitch propeller design process for a wind-powered car-carrier optimising for total energy consumption

Ioli Gypa [a,*], Marcus Jansson [b], Robert Gustafsson [b], Sofia Werner [c], Rickard Bensow [a]

[a] Chalmers University of Technology, Gothenburg, Sweden
[b] Kongsberg Maritime Sweden AB, Kristinehamn, Sweden
[c] SSPA Sweden AB, Gothenburg, Sweden

ARTICLE INFO

Keywords:
Marine propeller design
Wind-powered ship propulsion
Controllable-pitch propeller
Total energy consumption
Interactive optimisation
Cavitation evaluation

ABSTRACT

Wind-powered ship propulsion (WPSP) is the concept where the wind is the main source of thrust, while the traditional propulsion system operates when needed. This type of propulsion can lead to considerably reduced emissions, something that the shipping community is striving for. A well-known example of WPSP is the Oceanbird with the goal to cut emissions of up to 90%. In this study, the propeller design process for a wind-powered car-carrier (wPCC) such as the Oceanbird is investigated, what the various challenges of WPSP are and therefore how an automated optimisation procedure should be approached. A controllable-pitch propeller was selected as suitable propeller type for the operation of the wPCC, and various functions such as windmilling, feathering and harvesting have been explored. Regarding the optimisation procedure, an essential input is the definition of the operational profile, in order to determine the most important conditions for the route. The main objective of the optimisation is the minimisation of the total energy consumption (TEC), calculated based on a selection of conditions using the potential flow solver MPUF-3A. Cavitation has been evaluated by the blade designer, through an interactive optimisation method. The results showed that designing and optimising for the most highly loaded condition led to solutions with the lowest TEC.

1. Introduction

For years there has been an urgent need for reducing greenhouse gas (GHG) emissions globally. The goal of all industries in the current economical system has been to make profit, something that has led to the current levels of pollution. The transport industry alone was accountable for 27% of global emissions in 2019, a percentage which was temporarily reduced by 10% in 2020 due to the pandemic situation and thus the reduced need for transport (IEA, 2021a). However, in 2021 the transport demand rebounded, and the predictions showed a continuing demand for passenger and cargo transport (IEA, 2021b).

In 2012, the shipping industry was accountable for 2.2% of the global anthropogenic CO_2 emissions, with a projection of growing between 50% and 250% until 2050 (IMO Resolution MEPC.304(72), 2018). The International Maritime Organisation (IMO), in order to be in line with the ambitions of the 2015 Paris agreement (UNFCCC, 2015), has set a goal of reducing GHG emissions by 50% by 2050 compared to the emissions of 2008 (IMO Resolution MEPC.304(72), 2018). However, by comparing the global anthropogenic emissions, caused by the shipping industry, between 2008 and 2012, there has been an increase of 4.7%, according to the Fourth Greenhouse Gas Study 2020 (IMO, 2020). In 2021, with the aim to achieve a global net zero by 2050, the Clydebank Declaration for Green Shipping Corridors was signed by 22 countries, which handles the establishment of six green shipping corridors by 2050, where zero-emission routes between two or more ports will be created (COP26 Declaration, 2021). It is clear that the further development and utilisation of green technologies is needed for the decarbonisation of the transport sector.

Cleaner fuels, like biofuels, methanol, and hydrogen, for which there is currently extensive research and development (Carlton et al., 2013; Balcombe et al., 2019; Korberg et al., 2021), and alternative sources of energy, like wind or solar power, are the solutions that the shipping industry is increasingly choosing towards its decarbonisation. Wind-assisted ship propulsion (WASP), often combined with solar power technologies and cleaner fuels, is a concept preferred more and more by shipping companies, as a means to reduce emissions and save fuels costs. Commercial adoptions of WASP technologies for several types of vessels have been performed in recent years, all of which have been combined with a conventional propulsion system (Chou et al., 2021). In addition to this, a large amount of research has focused on WASP technologies, and more specifically on kites (Leloup et al., 2014,

* Corresponding author.
E-mail address: ioli.gypa@chalmers.se (I. Gypa).

https://doi.org/10.1016/j.oceaneng.2022.113426
Received 9 October 2022; Received in revised form 29 November 2022; Accepted 11 December 2022
Available online 4 January 2023

Abbreviations

CPP	Controllable-pitch propeller
FPP	Fixed-pitch propeller
GA	Genetic Algorithm
GWh/yr	GWatt*hours/year
IGA	Interactive Genetic Algorithm
MCR	Maximum Continuous Rating
NSGA-II	Non-dominated sorting genetic algorithm II
PCV	Parallel Coordinate Visualisation
SFC	Specific Fuel Consumption
TEC	Total Energy Consumption
TFC	Total Fuel Consumption
WASP	Wind-assisted ship propulsion
WPSP	Wind-powered ship propulsion

2016), Flettner rotors (Traut et al., 2014; Talluri et al., 2018; Tillig and Ringsberg, 2020; Seddiek and Ammar, 2021) and soft or rigid wingsails (Viola et al., 2015; Lu and Ringsberg, 2020). In these studies, different arrangements and sail area sizes of WASP technologies have been investigated, and they are often combined with other alternative sources of energy or fuels. Also, different weather conditions based on either real weather measurements or weather simulations were examined. The studies have shown a fuel cost reduction of 1%–50%, which is a wide range, but the results depend on the weather conditions, the type and route of the vessel and the WASP technology, thus each case is very specific. Also, the emission reduction calculation, if performed, is done in a different way in each study, by considering either the CO_2, or NO_x or SO_x emissions or all simultaneously.

The above mentioned studies use WASP solutions, where the main thrust comes from an engine, which is supported by the wind. Wind-powered ship propulsion (WPSP) has become more popular recently, where the thrust comes from the wind and is supported by an engine. Such a well-known case is the Oceanbird concept (The Oceanbird Concept, 2022), where the main thrust comes from the wind and the vessels adopting this concept will be equipped with wing rigs combined with a specially optimised sailing hull and the overall goal is to cut emissions by up to 90%.

A conventional propulsion system is nevertheless needed for propulsion with WASP and WPSP solutions. Although there is significant development in the area of wind propulsion (mostly on wing/sail technologies, hull design, weather route optimisation), there is very little research till now that has focused on the design and optimisation process of the propulsion system for wind-assisted/powered vessels. The propeller design and selection for such vessels is connected to many challenges that should be considered at an early design stage of the ship design spiral. We met some of these challenges in Gypa et al. (2022), where the KVLCC2 vessel was retrofitted with Flettner rotor sails and we investigated whether the existing fixed-pitch propeller (FPP) design was sufficient for covering the new operating needs and requirements, or whether a new design was needed. That study was not overly complex, with only wind-assistance, but it was a first effort towards clarifying the process on how to select, design and optimise a propeller for vessels that have been retrofitted with a WASP technology.

In the present study, we approach some further challenges for a more complex propeller design scenario for a newbuilding vessel. We select a baseline propeller and perform the blade design and optimisation for a controllable-pitch propeller (CPP) of the Oceanbird research concept for a wind-powered car-carrier (wPCC), which does a transatlantic crossing between two fixed destinations operating at constant speed. The wPCC is primarily designed for sailing and the propeller operates in a wide range of loading conditions, from very lightly loaded, when there is significant wind powering, up to highly loaded conditions, when there is a high sea state and the engine is needed for extra powering. As input to the study we have used velocity power predictions, performed by SSPA (Olsson et al., 2020), considering wind statistics from the Copernicus Climate Data Store (Copernicus Climate Data Store, 2022a). We follow a similar optimisation approach as in Gypa et al. (2022), where the aim was to minimise the total energy consumption (TEC) of the selected route. The cavitation of the propeller in the different operating conditions is controlled by the blade designer interactively, with the aid of the interactive genetic algorithms (IGAs), as part of an optimisation procedure, that had previously been presented by Gypa et al. (2021). In the present study, we must consider the parameter of the pitch as well and more specifically, the right pitch has to be selected for every operating condition since we are working with a CPP.

There is a research gap related to this issue of the design and optimisation process of marine propellers for WASP and WPSP vessels, although selecting the right propulsion system plays a significant role for the efficiency of the vessel and we believe that it should be part of the objectives and constraints of wind propulsion at an early design stage. The overall goal of this work is thus start filling this gap by proposing and describing a methodology for designing and optimising suitable propellers for wind-powered ships, in order to cover the demanding operating needs of WPSP.

This paper is organised as follows: We present a short background on the propeller design process and performance for WASP vessels in Section 2 and the challenges and limitations we face in wind propulsion in Section 3. The methodology is described in Section 4 and the case study in Section 5. The results are discussed in Section 6 and the figures of some additional results can be found in the Appendix. The paper finishes with the conclusions in Section 7.

2. Background on the propeller design process and performance for WASP vessels

A background on the propeller design process and performance for WASP vessels is summarised in this section. Molland and Hawksley (1985) made an assessment of the propeller performance for two WASP vessels, a coaster and a cargo ship. The performance of each vessel was assessed by either setting constant speed or constant power, coupled with various engine/gearbox types and propeller arrangements. In accordance with the results from both vessels, during the constant speed operation mode, for a single engine and a single screw installation, satisfactory efficiency was obtained by having an FPP. For twin engines and a single screw installation, CPP or a two-speed gearbox were preferable. When including the costs, a single engine and an FPP gave a better trade-off overall in both cases. During the constant power operation mode, engine power limits could not be reached as easily as in the constant speed operation mode, so again here an FPP was more suitable. When higher speed is needed, engines with small power margins can easily result in shaft speed limits though, which means lower thrust. A solution to this thrust decrease was the use of a CPP or a single engine with larger power margin.

Tillig and Ringsberg (2020) emphasised the high risk of potential pressure side cavitation for propellers that operate in a wide range of operating conditions, and therefore they suggested the use of a CPP for vessels that are equipped with WASP technologies with large sail areas.

In Gypa et al. (2022), we made a first effort on the propeller design and optimisation for a wind-assisted KVLCC2 that was retrofitted with six Flettner rotors. We investigated whether the existing propeller was sufficient or whether a new propeller design was needed for covering the new operating needs of the tanker, by setting as an objective the minimisation of the TEC. According to the results, the optimal propeller design offered approximately 0.9% reduction in TEC, compared to the baseline design, something that led to the conclusion that the existing propeller had acceptable performance and that a new retrofitted propeller was not economically motivated. We investigated five operating conditions, for varying propeller loads. Regarding cavitation, there was suction side cavitation within normal limits in all designs, and pressure side cavitation did not appear at all.

3. Challenges in propeller design for wind propulsion

3.1. Consequences of the wide operational profile

The main difference between conventional and wind propulsion is that although the weather conditions are always unpredictable, for wind propulsion we need to exploit the power of the wind. When designing vessels for conventional propulsion, we typically perform the propeller design work based on one operating condition, which is considered the design condition. With wind propulsion, the wind changes frequently, something that leads to a broader range of operating conditions for the vessel and to a wide load span for the propeller and the engine. Especially for wind-powered vessels, this span can be from 0 to 100% of the engine power. This results in a series of challenges, some of which we met in Gypa et al. (2022), and are briefly discussed here as well. In general, propellers for wind-propulsion are lightly loaded and they must operate well in off-design conditions.

The first thing to decide during the design process is what engine, gearbox and which propeller type are needed, based on the mission profile of the vessel. The selected engine and gearbox should cover all powering needs of the vessel, including high wind-powering, high sea state and normal calm water conditions. Then, the selection of an FPP or a CPP depends on several techno-economical factors, and each type is connected to different challenges, which are discussed in detail in Section 3.2.

Something that should be highlighted is that during the propeller-engine selection, in highly loaded conditions the engine should offer sufficient powering and the propeller should have a margin to the engine's upper torque limits. In lightly loaded conditions, the low shaft speed is connected to bearing lubrication issues on the shaft and there is a risk of the system reaching the engine's lower torque limits.

Another challenge is related to the optimal combination of propeller diameter and propeller speed. For conventional vessels the largest possible diameter is usually chosen, since we aim for the highest propeller efficiency at a certain rotational speed. For WASP/WPSP vessels that operate in several conditions with different loads, the aim is not necessarily highest propeller efficiency in one condition, but a low total energy consumption of all operating conditions combined. Therefore, the largest diameter might not fulfil the objective for those vessels. According to Andersson et al. (2021), a higher loaded propeller with 3%–4% smaller diameter together with a rudder system could perform better than with a larger diameter, for a conventional vessel. Thus, how to select the right combination of propeller diameter and propeller speed should be investigated for wind propulsion as well.

Overall, the biggest challenge is the broad range of operating conditions to consider, thus an accurate operational profile is the first thing needed, in order to carry out the blade design process. In wind propulsion, we should consider the whole operational profile during the optimisation, since the goal is to minimise emissions as much as possible for the entire route. Therefore the TEC and TFC (total fuel consumption) objectives, as presented in Gypa et al. (2022), should be the primary objectives, and in parallel it is necessary to control the cavitation behaviour, especially of the off-design conditions.

3.2. Selection of fixed-pitch or controllable-pitch propeller in wind propulsion

Depending on the size of the variation of the propeller load, the mission profile of the vessel, and the overall cost, the blade designers and the ship owner have to decide between an FPP or a CPP. In the propeller efficiency diagram of Fig. 1, an FPP is chosen for a fictive scenario, where there are three operating conditions, whose loading ranges from low to high. As depicted from the three points (η_1, η_2, η_3) on the efficiency (η) curve, after passing the peak of the curve, we slide off to the right of it, and then there is a quick drop in efficiency. However, when selecting a CPP instead of an FPP, there is the advantage of pitch

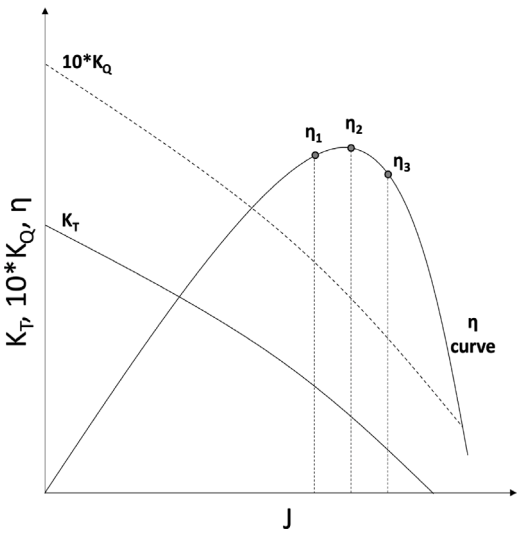

Fig. 1. Propeller efficiency diagram.

control that by changing the pitch, we can climb up to the peak of the curve, or at least be close to the peak.

In general, the design of a CPP is more complex and with a higher cost than an FPP. However, CPPs have the advantage that the full power can be utilised in various functions, like accelerating and stopping, quick manoeuvring and dynamic positioning among others (Dang et al., 2013), but some practical issues should be considered by the blade designers. First of all, the blades should not collide with each other, while passing from positive to negative pitch. The positioning of the blade on the blade foot should be done properly between the bolt holes and the blade overhang at the blade foot should be avoided so that stress concentration is prevented. Since the operational profile is usually very broad, the cavitation performance should be satisfactory in all conditions. For ducted CPPs, the tips of the blades should not touch the inner part of the duct (Dang et al., 2013).

Another important aspect in wind propulsion, especially for wind-powered vessels, is that when the wind-powering is considerably high and therefore the propeller is not operating, the propeller will be either windmilling or be in a feathered position (if a feathering CPP is selected), in order to reduce drag. The added resistance from the windmilling/feathering propeller should be considered and estimated early in the design process as well. Another aspect that can be considered is to harvest energy through a generator coupled to the windmilling propeller, adding further resistance but generating electricity at the same time.

Both propeller types offer different benefits. For wind-powered vessels, CPPs seem to be more beneficial, because the wind-powering is much larger than in WASP vessels. The possibility of feathering function is an important advantage as well. Therefore, we decided to move forward in this study with a CPP for the wPCC.

4. Method

4.1. Definition of operational profile for WPSP vessels

For the definition of the operational profile in wind propulsion, a key input is route simulations, which are provided for the vessel, often together with probability functions for the required delivered power, propeller revolutions, rudder–heel–leeway angles and thrust. Based on this input, the blade designer selects those conditions that can affect the blade design the most, conditions during which the vessels operate the most time and off-design conditions.

In WPSP, most of the time the vessel will operate either without using the propeller-engine system, or the propeller will be very lightly loaded. However, during harsh weather conditions, the engine will be operating without wind-support and the propeller will be very highly loaded. Hence, the designer always needs to consider the torque limit of the engine when working with the different operating conditions in the design process

4.2. CPP selection

When the designers are provided with the most important information for the project and the main requirements for the propeller and mission profile of the vessel, they decide on the propeller type and the engine requirement. To start the blade design process, the following are required:

- Engine solution
- Engine limit curve
- CPP data at off-design conditions

The last point is especially important when we move so far off-design as we do in this study. In an FPP scenario, we would use an open water design pitch curve, but for CPP, we need additional information that regards the pitch settings for off-design conditions; especially in WPSP, very wide pitch settings are needed. This information is usually given by propeller series data (Carlton, 2018).

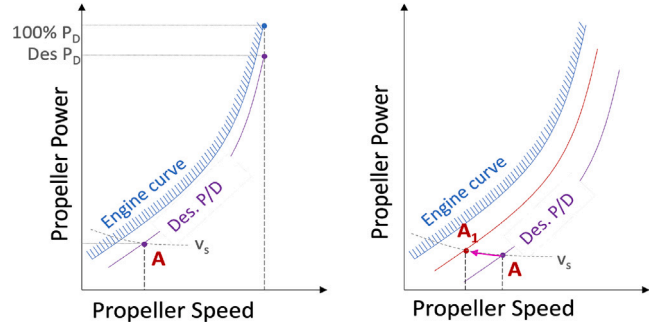

Fig. 2. PDn diagram.

The performance assessment of CPPs is usually done with the aid of PDn (propeller power–propeller speed) diagrams. In Fig. 2, two such diagrams that represent two operating conditions are shown. The diagram on the left presents a condition A, where the 100% of the loading comes from the propeller (no wind powering). This is considered the baseline design of a fictive scenario, where there is a design point at 90% of maximum continuous rating (MCR) and the pitch at this point is the design pitch. The diagram on the right presents another condition A, where there is part wind-powering. As depicted from the plot, the design pitch moves to the right and is no longer optimum for this condition. Thus, by increasing the pitch, we move the operating condition from A to A_1, and we manage to increase the efficiency for a given ship speed and at the same time maintain a torque margin to the engine curve. Note that by increasing the pitch, one can get closer to an optimum efficiency, but one should still maintain a torque margin to the engine curve. The starting point for selecting the pitch is by using data from propeller series; then the selected pitch is corrected to ensure high efficiency and maintain a torque margin to the engine curve.

Based on the propeller type, the main characteristics of the propeller and the pitch settings, the blade designers create a baseline propeller design for each one of the operating conditions, which is a potential starting point of the optimisation.

4.3. Optimisation method

In this study, we follow a similar optimisation approach as in Gypa et al. (2022). The main idea of the optimisation process is that a good baseline design (for each one of the selected conditions) is created and the goal is to improve the performance of this design by using an optimisation tool. The initial blade design is referred to as baseline and it is the starting point of the optimisation.

The designer selects the most important geometrical characteristics that affect the propeller performance (e.g. P/D, camber etc.), and sets them as design variables, which vary between some pre-defined limits during the optimisation, and form the design space. By modifying the design variables, new propeller geometries are created. The optimisation algorithm searches for the best solutions (propeller geometries) in this design space, according to the objectives of the specific problem.

The curves of the distributions of all design variables are represented by B-splines in our tools. An example of a P/D curve, along with the control points and the pre-set ranges for the optimisation, is presented in Fig. 3. The dashed green line represents the P/D curve of the baseline design. The top and bottom red lines represent the minimum and maximum curves, after defining the range of each control point of each design variable. It is also shown that a control point at approximately 0.59R has been moved and the resulting curve is represented by the bold green curve. Since more than one control points are usually modified at different blade sections, the curve is first modified at one blade section, then for the next ones, so that a smooth final curve is obtained.

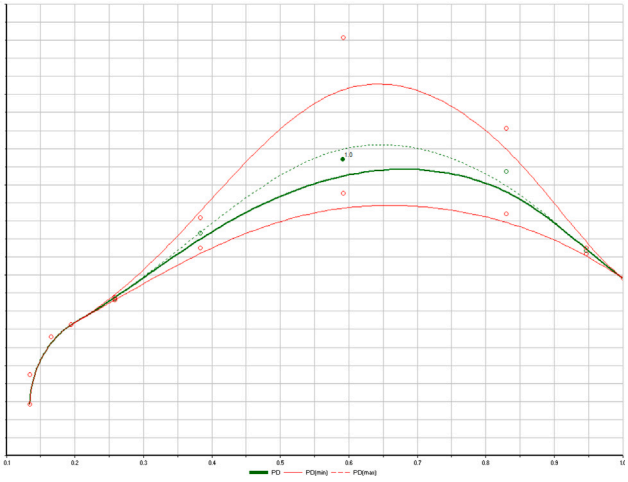

Fig. 3. Range of minimum and maximum P/D curves.

The objectives and constraints of the optimisation problem are defined by the designer as well and are usually related to propeller efficiency, cavitation, pressure pulses and strength, depending on the mission and operational profile of the vessel. Two new objectives were introduced in Gypa et al. (2022), the TEC (total energy consumption) and the TFC (total fuel consumption). The overall aim with our approach is to minimise the TEC or TFC for the weather scenario, while maintaining the required thrust for all operating conditions. In combination with the TEC or TFC objectives, the designer can select any of the other usual objectives, depending on the optimisation problem. The TEC is calculated as follows:

$$total\ energy\ consumption = \sum_{i=1}^{n} P_{D_i} * t_i, \tag{1}$$

where P_{D_i} is the delivered power to the propeller for each condition and t_i is the operating time for each condition.

When there is detailed engine information with specific fuel consumption available, it is possible to calculate the TFC, according to:

$$total\ fuel\ consumption = \sum_{i=1}^{n} P_{D_i} * t_i * SFC_i, \tag{2}$$

where SFC_i is the specific fuel consumption for each operating condition.

When the optimisation setup is defined, an optimisation process starts by running the optimisation algorithm, new designs are produced by modifying the design variables and the objectives drive the optimisation towards a design space with high performance and the lowest TEC or TFC for all the selected operating conditions.

4.4. Computational tools

The hydrodynamic analysis tool we use in this study for the prediction of the propeller performance and the sheet cavitation is the vortex lattice method code MPUF-3A (He et al., 2010). The geometry of the propeller blade is represented by a lattice of discrete vortices and sources, distributed on the mean camber surface of the blade (Vesting, 2015). The kinematic boundary condition on the blade surface is considered for the strength of the vortices, where the wetted portion of the blade surface is impermeable to the fluid, and the Kutta condition is applied at the trailing edge, where the flow should leave the trailing edge in a tangential direction (Lee, 1979).

The cavitation prediction is based on an iterative process, according to Kerwin et al. (1986), where a 2D cavitating profile section is considered and the cavity interface is represented by including sources whose strengths must be solved for in each time step. For the 3D solution, the cavity length is adjusted for all sections for the time step. This is done by considering radial stripes of the blade that are solved until convergence is accomplished, starting from the hub until the tip of the blade and back. Each blade section is thus constructed by this set of stripes in the flow field by combining the undisturbed inflow and the induced flow of the other stripes. The solutions are computed for only one blade, the key-blade, in order to save computational cost. Subsequently, it is assumed that the strengths of the vortices and sources on the other blades correspond to those that were calculated for the key-blade (Vesting, 2015) at that position. Additionally, in this study a fixed blade wake is being taken into consideration. MPUF-3A includes also the effect of the hub, the wake alignment in circumferentially averaged inflow with an arbitrary shaft inclination angle and the nonlinear thickness loading coupling (Kinnas et al., 2003).

4.5. Cavitation evaluation

An interactive optimisation methodology has been presented in Gypa et al. (2021), where cavitation was interactively controlled by the blade designer during the optimisation. More specifically, IGAs were used, in order to guide the optimisation algorithm towards areas of the design space with high performance and satisfactory cavitation characteristics, based on the preference of the designer. According to this method, at the end of an optimisation run, images of the cavity shape on the blade of the designs are presented to the blade designer and the designer evaluates them as “accepted” or “rejected”, based on the project’s requirements and the designer’s preference and experience. Then the optimisation continues, if needed, with the designs that were “accepted” by the blade designer, so that there is convergence towards areas of the design space that have accepted cavitation, following the preference of the designer, and high performance, according to the objectives of the optimisation.

This method is flexible and the interactivity can be used at any stage of the optimisation, when needed. In Gypa et al. (2021), there were several intermediate stages during the optimisation, where the cavitation behaviour was displayed and the designer assessed it manually. During the optimisation in Gypa et al. (2022), we selected to display the cavitation shape at the end of the optimisation procedure, since all designs had nearly the same cavity shapes, which did not require assessment during more intermediate stages.

5. wPCC case study

The case study is based on the Oceanbird research concept for a wPCC, similar as in Fig. 4. The specific case is very interesting for our research, since there is no other study focusing on the propeller design and optimisation for such vessels, where the propeller loading varies so much, and an efficient propeller is needed for the whole operational profile. The wPCC has a length of 200 m, the displacement is 30,000 tons and the cargo is 7000 cars. It follows a route between two fixed destinations (Southampton-New York) across the Atlantic Ocean in 12 days, for a constant speed of 10 knots.

It is a twin screw vessel with open shafts and brackets. The hull is shown in Fig. 5 and has specifically been optimised for sailing. The wPCC in this study is equipped with four identical, rigid, single element wing sails, each with a plan form area of 1844 m^2. The wings are placed along the centreline of the vessel and they are free to rotate 360°, while the spacing allows for independent rotation. More information on the sails can be found in Malmek et al. (2020).

Fig. 4. The Oceanbird concept - wPCC.

Fig. 5. Hull of twin-screw wPCC.

SSPA performed resistance and propulsion tests, load variation tests, CFD simulations at a matrix of drift and rudder angles, and route predictions and provided us with the results (Werner, 2021) that are the input needed for our analysis. We aim to design and optimise an efficient CPP, that will cover all operating needs of the vessel and will minimise the TEC of the entire route. The following assumptions have been made throughout this study:

- We have assumed a leeway angle of 0°. According to the report from Werner (2021), the average leeway angle is 2°, but for this particular hull, having been optimised for sailing, the leeway angle of the vessel did not have a significant effect on the wake.
- When the engine is used, with or without the sails, the speed is constant at 10 knots. However, in extreme harsh weather, the crew might reduce speed below 10 knots, similarly as in conventional vessels, but this is something that is not studied in this work.
- The required thrust ranges between 0 kN up to approximately 800 kN. In the present study, it is assumed that the engine load can vary 0%–100%, even if this might not be possible in reality.

5.1. Operational profile

SSPA provided us with the route predictions, which were performed by using a velocity prediction programme and a voyage simulation tool (Olsson et al., 2020) for the route Southampton-New York and the wind statistics were obtained from the Copernicus Climate Data Store (Copernicus Climate Data Store, 2022a). The speed is assumed to be constant at 10 knots.

Probability distributions for the thrust and time of the entire route were provided by SSPA. The vessel is in sailing mode 50% of the time, with the wind providing the entire powering and the engine and propulsion system not operating. The remaining 50% of the time, the powering is provided by both the wind and the engine. There is a wide operational profile, but since it would be time-consuming to include the entire profile in our design and optimisation process, five operating conditions have been selected. The propeller load for these conditions ranges from very light to high. The following conditions have been selected:

- Condition 1: T_1 = 50 kN
- Condition 2: T_2 = 90 kN
- Condition 3: T_3 = 190 kN
- Condition 4: T_4 = 260 kN
- Condition 5: T_5 = 390 kN

The probability distribution is then normalised for the five conditions only and subsequently the time for each condition is computed. The operating time of operational profile 1, which will be mentioned as OP_1, is shown in Table 1. In order to account for that the weather conditions are unpredictable, we investigate the performance of the designs also in a second different operational profile to test the robustness of the process. In this profile, 193 h of the yearly hours are spent in conditions 1 and 2, which are more lightly loaded, and are deducted from conditions 4 and 5, which are more highly loaded. So in the operational profile 2 (OP_2), the wind is expected to be more advantageous for the vessel or the weather conditions not as harsh as in OP_1. The operating time of OP_2 is shown in Table 2. In both profiles, 50% of the time the propeller-engine system is not used, since there is full wind-powering.

Table 1
Operational profile 1.

Condition	% of time	Hours/year
1	9.8%	858
2	13.8%	1209
3	12.2%	1069
4	9.2%	806
5	5%	438

Table 2
Operational profile 2.

Condition	% of time	Hours/year
1	10.3%	902
2	15.5%	1358
3	12.2%	1069
4	7.5%	657
5	4.5%	394

5.2. Wake input

CFD simulations for the wake were performed and provided by SSPA. We used as input for the design of the baseline and the optimisation a fixed wake for a leeway angle of 0 degrees. As shown in Fig. 6, the axial component is quite homogeneous, but there is also a strong diagonal component with some smooth variation in one direction.

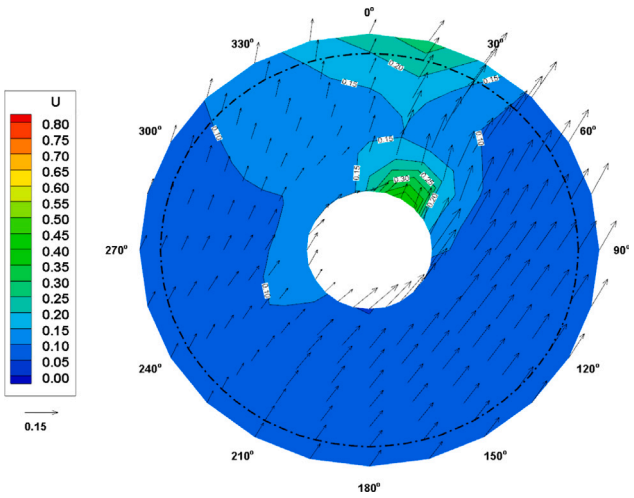

Fig. 6. Wakefield.

5.3. CPP baseline design

In order to start creating the baseline design, an engine solution, an engine curve and CPP series data are needed. As mentioned earlier, it is assumed that the engine load can vary 0%–100%. We use a simplified engine limit curve: $P = n^3$, where P is the shaft power and n the shaft speed, which is shown in Fig. 7.

Moreover, the baseline design is based on a stock propeller of the Wageningen C-series (Dang et al., 2013), in order to select the most suitable pitch settings for each condition that will offer the optimal performance. An example of three different C4-40 series propeller models at their design pitch settings are shown in Fig. 8.

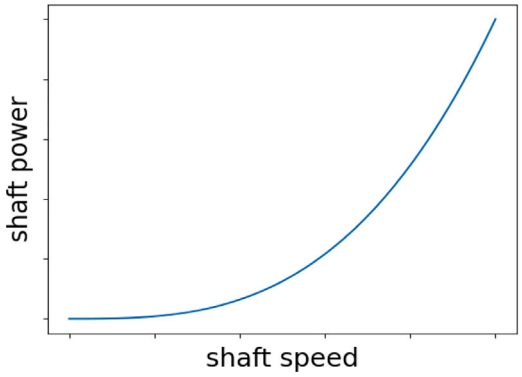

Fig. 7. Engine curve.

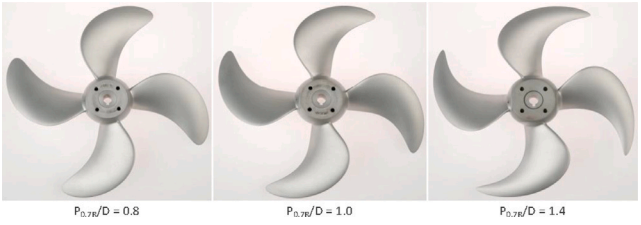

Fig. 8. Three C4-40 series propeller models at design pitch settings (Dang et al., 2013).

Based on the Wageningen C-series, we selected the most suitable pitch settings for each one of the conditions, and then we corrected them in order to attain optimal efficiency, while maintaining a 5% torque margin to the engine curve for the constant speed of 10 knots. In Fig. 9, the PDn diagrams of three conditions of the wPCC are shown, when the propeller operates 100% in calm water (typical design

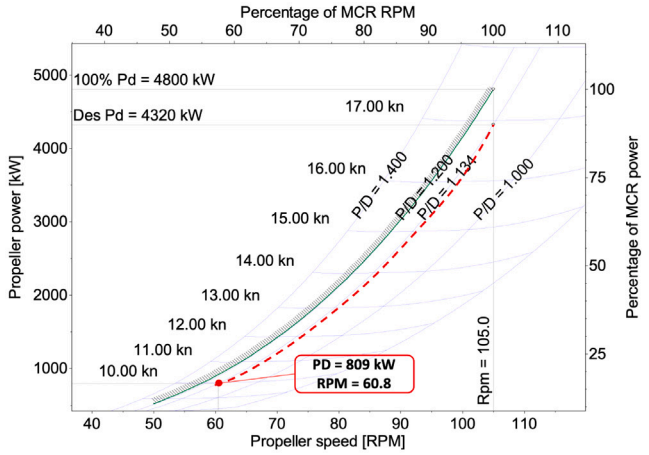

(a) Propeller 100%

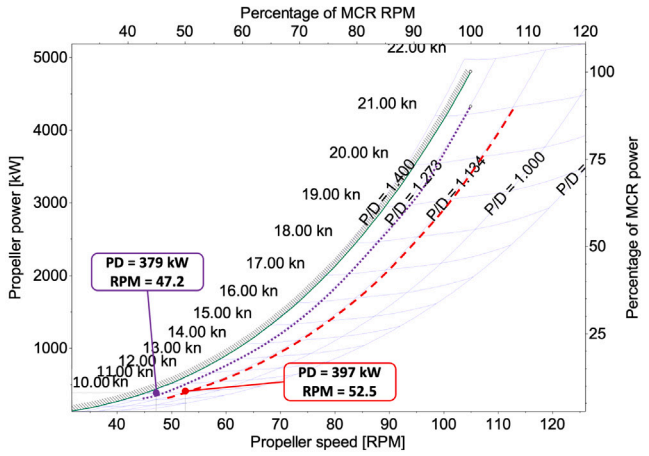

(b) Motor - Sailing

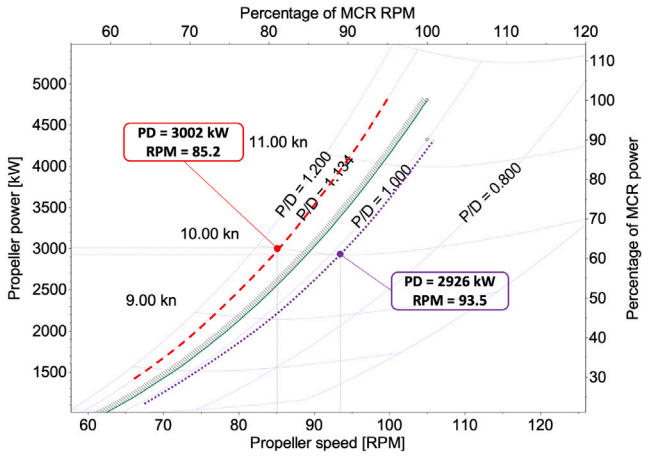

(c) Motor against waves

Fig. 9. PDn diagrams for three conditions.

condition), when there is motor — sailing simultaneously and when the motor operates against waves (high sea state). In Fig. 9(a), where there is 100% propeller load, the MCR (maximum continuous rating), is the point at 100% of the powering. The design point is at 90% and a design pitch that offers a reasonable margin to the engine limit curve. For the constant speed of 10 knots, one observes that the propeller is very lightly loaded for a total engine power of 10 MW. This means that at the service condition of 10 knots, the system operates below the idle speed

Table 3
Settings of the five selected conditions.

Condition	Thrust [kN]	n [rpm]	P_D [kW]	P/D
1	50	34.5	145	1.86
2	90	42.1	259	1.55
3	190	53.9	571	1.36
4	260	60.8	809	1.26
5	390	71.4	1282	1.17

(shaft speed below 60%) of a typical diesel engine. Fig. 9(b) represents a motor-sailing condition and it is evident that the design pitch moves to the right, thus it is no longer optimum for this condition. By increasing the pitch (to the dotted curve), the efficiency increases by 4% (with a 5% torque margin). The pitch changes significantly, from 1.134 to 1.273, but this change is reasonable for a CPP and the shaft speed is 47.2 rpm; thus there is no risk of having bearing lubrication issues according to a threshold of 20–25 rpm, set by experience (Kongsberg hydrodynamic design team, 2022). Fig. 9(c) represents a motor against waves condition, where the design pitch moves to the left beyond the engine curve. Therefore, we decrease the pitch (towards the dotted curve) to maintain the 5% torque margin and the speed at 10 knots.

This process is repeated for the five conditions that form the operational profile of the vessel and in Table 3, the different settings for each condition are presented. The P/D of conditions 1 and 2, which are equal to 1.86 and 1.55 respectively, exceed the C-series test range (P/D_1) and the mechanical limit of the selected hub for this study (P/D_2). Those pitch settings are used in this study though, but it should be kept in mind that the obtained efficiency will be over-predicted.

5.4. Optimisation set-up

The geometrical characteristics of the CPP are shown in Table 4. The P0.7/D is equal to 1.134 for the design condition, when the propeller operates 100% at calm water. The selected design variables, which are described below, have a variation range of ±10% from the values of the baseline design.

Table 4
WPCC propeller data.

Propeller diameter	(D)	5000 mm
Hub diameter	(d)	1020 mm
Number of blades	(Z)	4
Expanded blade area ratio	(AE/A0)	0.4
Pitch ratio at 0.70R	(P0.7/D)	1.134

- Pitch over propeller diameter (P/D) at the radial positions: 0.134R (blade section extended below hub radius), 0.7R and 1.0R.
- Camber (FM) at the radial positions of 0.134R, 0.7R and 0.95R.
- Chord length (L) at 0.9R.

The overall goal is to decrease emissions as much as possible, so the TEC or TFC are the principal objectives that drive the optimisation. The detailed engine information has not been provided for this study, which is required for the TFC, thus we will use the TEC as the objective, and it will be a single-objective optimisation since there are no other major goals; constraints are discussed below.

We perform a number of separate optimisation runs that will have the baseline design as starting point for each one of the conditions. The condition for which we design is called design condition and the remaining four are called analysis conditions. Condition 1 or C_1 (T_1 = 50 kN) could not be set as a feasible design condition, due to mechanical constraints related to the hub and its crank angles. Due to the high design pitch of the specific condition, it was not possible to ensure sufficient angle margins. So the design conditions are conditions 2, 3, 4 and 5 (C_2, C_3, C_4, C_5), each one of them have a different baseline design and we will perform an independent optimisation run, which we

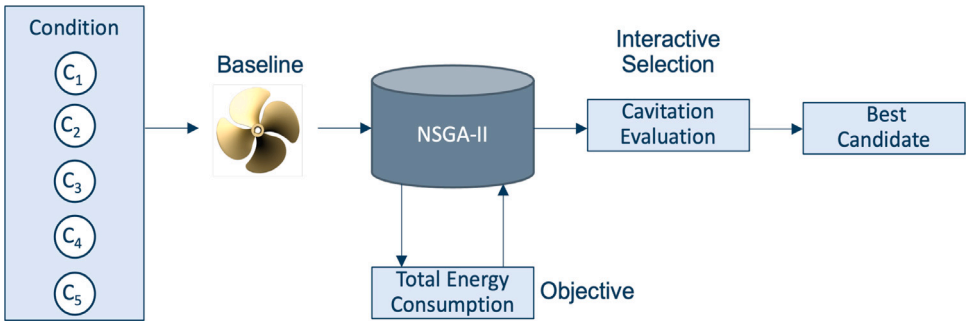

Fig. 10. Optimisation flowchart.

refer to as R_2, R_3, R_4 and R_5. Depending on the operational profile and in order to distinguish them, they are mentioned as R_{2-OP1} or R_{2-OP2} etc. The reason we perform independent optimisation runs is that we have a different baseline design as a starting point, thus the design space differs and each run will lead to a different optimal design. At the end of this process, we will gain more knowledge on which starting point seems to be the best for wind-powered vessels with off-design conditions, and most probably doing independent optimisation runs will not be necessary. The optimisation flowchart is shown in Fig. 10.

We perform also some additional optimisation runs for the design condition C_5 for both operational profiles, where we widen the limits of the design variables. For OP_1 we perform two additional runs, the R_{5b-OP1} and the R_{5c-OP1}. For R_{5b-OP1}, the pitch and camber variables have a variation range of ±20% and the chord length has a range of −40% and +20% from the baseline value. For R_{5c-OP1}, the pitch and camber are the same as in R_{5b-OP1}, but for the chord length we add one more control point at 0.7R, with limits −10% and +20% from the baseline value, while the chord length at 0.9R has limits −25% and +20% from the baseline value. For OP_2 we perform one additional run, the R_{5b-OP2}, which has the same design variable ranges as R_{5c-OP1}. The goal with the additional runs is to investigate whether the wider range of the design variables will lead us to areas of the design space with lower TEC.

There is one quantitative constraint in this problem, the thrust coefficient K_T and its limits have been set so as to achieve a ±1 kN from the values of the baseline thrust. The flowchart of this part of the optimisation process is shown in Fig. 11, according to which we start the optimisation with the baseline geometry of one condition (e.g. C_2). The limits of the design space have been set by the blade designer prior to the optimisation and the NSGA-II selects one value for each design variable. In the next part, the algorithm checks whether an acceptable thrust for C_2 is obtained. If the thrust is not within the required limits of ±1 kN from the baseline thrust, the pitch curve (P/D curve) is iteratively adjusted, at 0.7R and within a separately specified range. This then overrides the design space parameters to try and fulfil the K_T criterion. After obtaining an acceptable thrust for the design condition, the thrust of the analysis conditions is checked and if not satisfying, the shaft speed is adjusted until we obtain an acceptable thrust. If this does not work, the individual is disqualified and excluded. Then the delivered power of all conditions is calculated, in order to calculate the TEC, which involves the energy consumption from both design and analysis conditions. This process is repeated until all designs of the current population are created and then the run either finishes or we move on to the next generation. In this way, we know that the designs we have created have an acceptable thrust for all involved conditions, and the TEC is calculated correctly.

For OP_1 the optimisation runs R_{2-OP1}-R_{5b-OP1} are performed for 10 generations and each generation has 100 individuals. The run R_{5c-OP1} is performed for 20 generations, with 100 individuals per generation. The optimisation runs of OP_2 R_{2-OP2} - R_{5-OP2} are performed for 25 generations of 100 individuals each and the run R_{5b-OP2} is performed

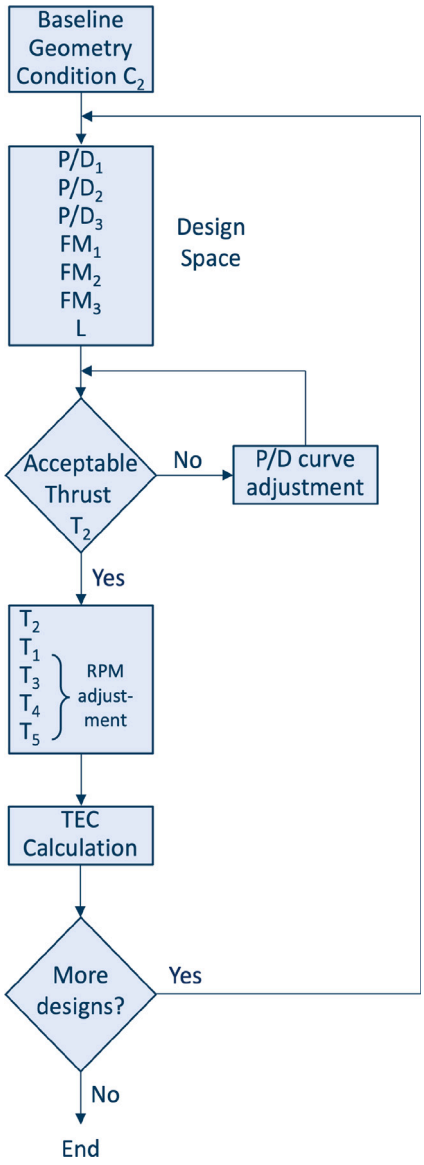

Fig. 11. Optimisation process including the pitch adjustment.

for 35 generations of 100 individuals each. The crossover operator is set to 0.75 and the mutation to 0.15 for all runs.

Cavitation is handled as a qualitative constraint in this study. The designer looks at the cavitation pictures that are displayed on the screen and accepts or rejects them based on their preference on this project. As shown in Fig. 10, in this study the cavitation is assessed at the end

of the optimisation runs, because the baseline designs have almost no cavitation in all conditions, due to the fact that it is a newbuilding vessel and the hull has specifically been optimised for sailing. However, as mentioned earlier in Section 4.5, the manual cavitation evaluation can be part of the optimisation loop in scenarios that cavitation appears and must be controlled.

6. Results & discussion

6.1. Propeller operation during 100% sailing

According to the prediction of the operational profile, 50% of the time the vessel will be in pure sailing condition and the propeller will be inactive, so there is the question of what happens with the propeller during the sailing condition. There are three possibilities, depending on the options of the selected CPP and hub. The propeller will be in windmilling or feathering position or in harvesting operation.

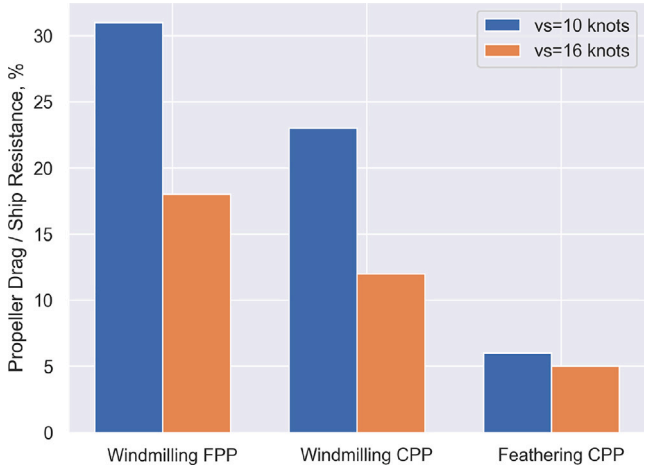

Fig. 12. Propeller drag over ship resistance in windmilling and feathering positions.

Windmilling means that the propeller does not operate and is rotated only by the flow of the water, while a feathered propeller is the propeller whose blades are locked in the lowest drag position. In Fig. 12, the propeller drag over the ship resistance is presented for windmilling FPP, windmilling CPP and feathering CPP, for two ship speeds of 10 knots (blue) and 16 knots (orange). As depicted from the plot, the drag over the ship resistance of the windmilling FPP (P0.7/D = 1.134) is significant, with over 30% at 10 knots and 18% at 16 knots. For the windmilling CPP (P0.7/D = 1.399), the drag is reduced to 23% and 12% at 10 and 16 knots respectively. The best option of the three is to have a feathering CPP (if there is this option), where the drag reduces to 6% and 5% at 10 and 16 knots respectively.

Another possibility for the propeller is to use it for harvesting, i.e. use the propeller for generating energy when the wind conditions are favourable. We have done this investigation for two pitch settings (P0.7/D = 1.134 & P0.7/D = 1.399) and for the same two ship speeds of 10 and 16 knots as before. The efficiency of the harvesting propeller for the 10 knots is shown in Fig. 13, with the P0.7/D = 1.134 and P0.7/D = 1.399 in 13(a) and 13(b) respectively. The mechanical losses are assumed to be 4% of the maximum torque, which is considered reasonable for this type of shaft line system with gearbox (Kongsberg hydrodynamic design team, 2022). The propeller efficiency is shown in the figures without (blue colour) and with (orange colour) the shaft losses, for different shaft speeds. It is evident that with both pitch settings, the effect of the shaft losses on the harvesting propeller is significant . At the ship speed of 16 knots, the efficiency drops when not including the shaft losses, but when included, it is almost the same as at the ship speed of 10 knots (see Fig. 14).

These results are based on the outcome of open water model test data, thus it should be taken into consideration that scale effects most

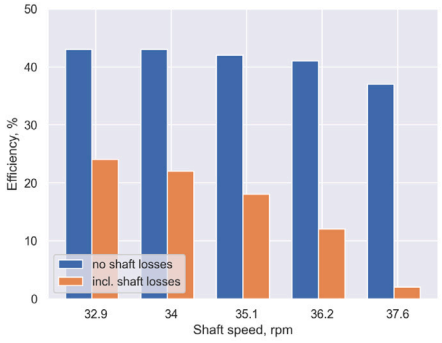

(a) P/D = 1.134

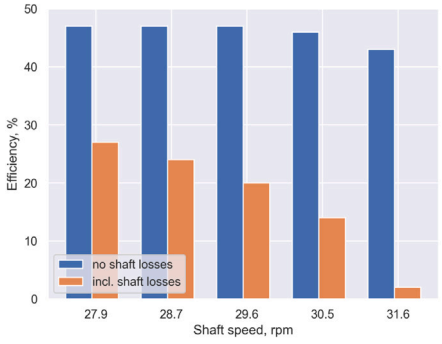

(b) P/D = 1.399

Fig. 13. Harvesting at 10 knots.

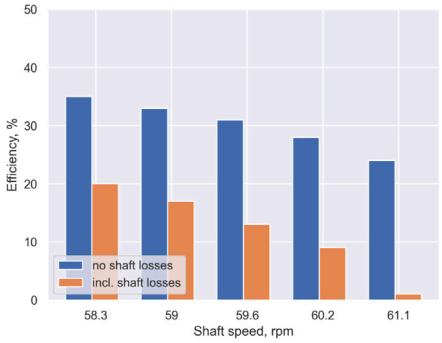

(a) P/D = 1.134

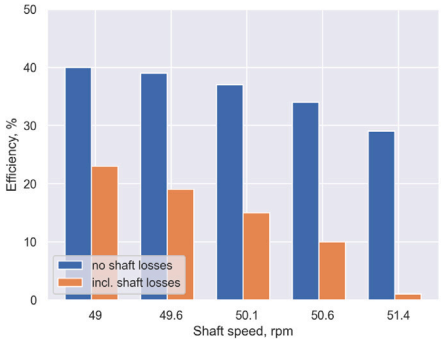

(b) P/D = 1.399

Fig. 14. Harvesting at 16 knots.

probably exist. Due to the unusual position of the propeller, which is windmilling or feathering, and the fact that the propeller operates at very low shaft speeds, there is insufficient validation data of operation in full scale in such conditions. In addition to this, there are just a few actual installations of harvesting propellers, mainly for smaller vessels.

From this analysis and for the specific study, there are specific limitations connected to the engine and shaft speed. The idle speed of a normal diesel engine is 60% of the nominal shaft speed; in the condition at 10 knots when only the propeller operates, the shaft speed is below 60% of the nominal shaft speed. As previously mentioned, the propeller shaft speed should be above 20–25 rpm in order to avoid bearing lubrication issues. This is covered in this particular study for all conditions that the propeller operates, but in case of windmilling, the shaft speed should be checked. If the propeller would be used as a turbine, then the frictional losses should be minimised, since otherwise a significant part of the generated power could be lost.

6.2. Optimisation

The results of the optimisation for all runs and both operational profiles are discussed in this section. We present results related to the energy consumption of the baseline designs of every run, the convergence of the optimisation algorithm, the geometrical characteristics of the optimal designs and how these perform in different operational profiles, how the design space of the optimisation has been searched and finally the cavitation characteristics of the obtained designs. Additional plots related to the design space can be found in the Appendix.

6.2.1. Energy consumption

The energy consumption of the baseline designs for OP_1 and OP_2 is shown in Figs. 15(a) and 15(b). The x-axis of the plots represents the design condition and the y-axis the energy consumption. Each bar represents one of the four analysis conditions, together with the one design condition. The purpose of these plots is to show how much of the energy consumption of each condition contributes to the TEC and how the TEC is affected by the baseline of the design condition.

For both operational profiles, the lowest TEC is obtained for the baseline design of condition C_5. Regarding the optimisation procedure, it is therefore reasonable to later obtain the optimal design when we have this baseline design as a starting point. However, due to the stochastic nature of the GA, we cannot be sure about this result, and accordingly we have performed independent optimisation runs, which have as starting points the different baselines from the four design conditions.

By observing the energy consumption of each analysis condition independently, in OP_1, there is lowest energy consumption for the analysis condition C_1, where the P_D is very low (approximately 280 kN) and the duration is 858 h/year. The highest energy consumption is at analysis condition C_4, where the P_D is high (approximately 1900 kN) and the duration is 806 h/year, almost the same as in condition C_1. Clearly the much higher value of P_D affects the energy consumption. In OP_2, the lowest energy consumption is again obtained at the analysis condition C_1, although the duration is 902 h/year, 44 more hours compared to OP_1, for the same P_D. The highest energy consumption is obtained at analysis condition C_3, which has a duration of 1069 h/year, the same as in OP1 and for $P_D \approx 1275$ kN. However, in this OP, the duration of analysis condition C_4 has been reduced by 149 h and C_5 by 44 h, therefore the energy consumption was reduced.

6.2.2. Convergence

The convergence of the optimisation for the four runs of OP_1 is shown in Fig. 16(a). First of all, the lowest TEC is obtained by the optimisation R_{5-OP1}, and is represented by the red continuous line. Moreover, a common characteristic in all convergence lines is that there is a big drop in TEC at the first generation, and then the TEC reduces more gradually. The runs R_{2-OP1} and R_{4-OP1} converge early towards

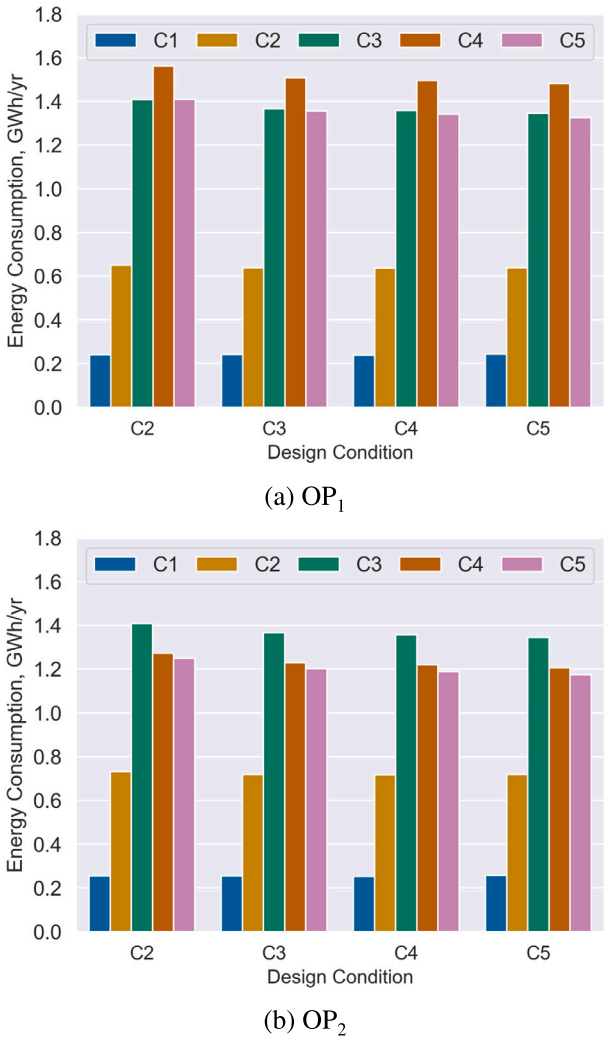

Fig. 15. Energy consumption for the baseline designs prior to the optimisation.

the optimal solution, while it seems that for R_{3-OP1}, the algorithm has not converged towards one solution and could be run for longer time.

The convergence of the runs R_{5b-OP1} and R_{5c-OP1} with the wider limits at the design variables, together with the R_{5-OP1}, are presented in Fig. 16(b). As depicted from the convergence line (orange) of R_{5b-OP1} in the plot, there is a very large drop in TEC from the first generation. The green convergence line of R_{5c-OP1} shows that the TEC is somewhere between the initial run R_{5-OP1} and the run with the wider limits R_{5b-OP1}. This last run has not converged towards one solution, it could be run for even more generations. However, since the computational cost is very high and the TEC improvement very small at this stage of the evolution of the optimisation, we did not perform a longer run.

Similar results are obtained with the OP_2, as presented in Fig. 17. The optimisation of every condition has been run for 25 generations, since some runs of OP_1 did not converge after 10 generations. Here all runs converged towards one solution. Similarly as with OP_1, the lowest TEC was achieved with the run R_{5-OP2}. For the optimisation run R_{5b-OP2}, the TEC reduces even more and it seems that if the optimisation had continued, maybe even lower TEC would be achieved. However, one should think whether it is worth running the optimisation even longer for such small TEC improvements, when the computational cost is very high.

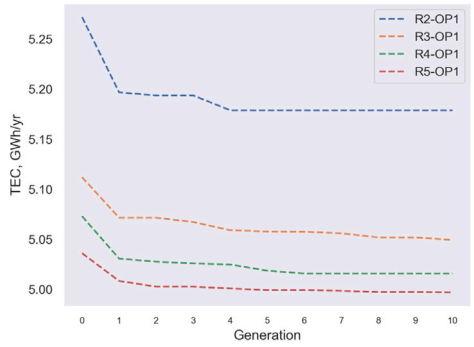

(a) All runs

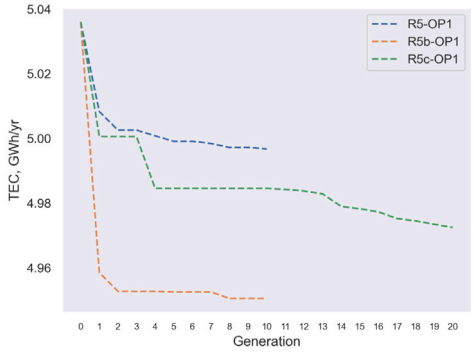

(b) R_{5-OP1}

Fig. 16. Optimisation convergence — OP_1.

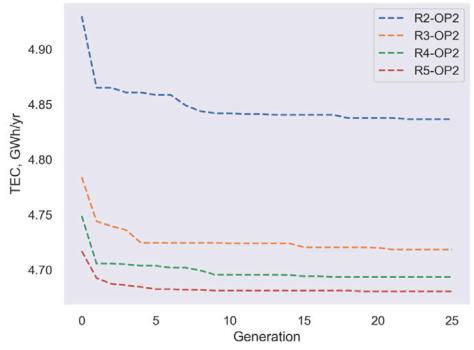

(a) All runs

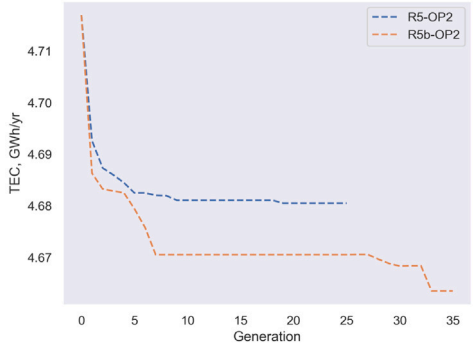

(b) R_{5-OP2}

Fig. 17. Optimisation convergence — OP_2.

Table 5
Optimal solutions - OP_1.

Run	TEC - Basel.	TEC - Opt.	Difference
R_{2-OP1}	5.27	5.18	−1.77%
R_{3-OP1}	5.11	5.05	−1.23%
R_{4-OP1}	5.07	5.02	−1.13%
R_{5-OP1}	5.04	4.99	−0.78%
R_{5b-OP1}	5.04	4.95	−1.69%
R_{5c-OP1}	5.04	4.97	−1.26%

Table 6
Optimal solutions - OP_2.

Run	TEC - Basel.	TEC - Opt.	Difference
R_{2-OP2}	4.93	4.84	−1.89%
R_{3-OP2}	4.78	4.72	−1.37%
R_{4-OP2}	4.75	4.69	−1.17%
R_{5-OP2}	4.72	4.68	−0.77%
R_{5b-OP2}	4.72	4.66	−1.13%

6.2.3. Optimal designs

In OP_1, as presented in Table 5, the lowest TEC, which is measured in GWh/yr is obtained by the optimisation run R_{5b-OP1}. The largest reduction in TEC, when compared to the baseline, occurred with R_{2-OP1}, which offered a reduction of 1.77%.

The geometry of the best individuals of the six runs are presented in Fig. 18. One observes directly in Fig. 18(b) that the design depicted from R_{5b-OP1} with the wider limits would not be a feasible propeller geometry, due to the weird blade shape.

This is evident also in Fig. 19, where the chord length over the diameter (C/D) of the best designs of the six runs is presented. The C/D curves of the designs from R_{2-OP1}-R_{5-OP1} are almost the same. The C/D curve obtained from R_{5b-OP1} has an S-shape at 0.4–0.98R. The C/D curve obtained from R_{5c-OP1} looks like a straight line at 0.7–0.98R, which means that the chord length reduction did not take place smoothly. Manual modifications would be required by the blade designer to smooth the curve, if this geometry would be selected as optimal.

The detailed geometry (values of the design variables) of the six optimal designs of the six runs is presented in the parallel coordinate visualisation (PCV) of Fig. 20. The first seven axes represent the range of the seven design variables of this problem and the last axis shows the operating condition. The colour scale represents the TEC and its colour variation depends on how low or high the value of TEC is. Each line represents one optimal design and shows the values of its design variables and which operating condition they represent and the colour of the line depends on the TEC value.

The values of the design variables of the optimal design of R_{2-OP1}, which offered the highest TEC, are the complete opposite of the values of the design variables of the other runs, with very high values in pitch and very low values in camber. The other optimal designs have a tendency of decreasing the pitch values and increasing the camber values. The three optimal designs of R_{5-OP1}, R_{5b-OP1} and R_{5c-OP1} had almost the same values for pitch and camber, while for the chord length they had values closer to their minimum limits (which differed in every run).

The same process has been performed in order to present the results for the best designs of OP_2 in Table 6 and in Figs. 21–22. Again the lowest TEC is obtained from R_{5b-OP2}. The geometries of the best individuals of the five runs in Fig. 21 are all feasible. In the PCV of the five best individuals of Fig. 22, the values of the design variables for R_{2-OP2}, similarly as in OP_1, are opposite from the values of the other runs. The two best designs from R_{5-OP2} and R_{5b-OP2} have almost the same values in pitch and camber. Again here, the chord length of all designs is almost at the minimum limits. Note that the minimum value of the chord length for the run R_{5-OP2} differs due to the pre-set wider range of the variables.

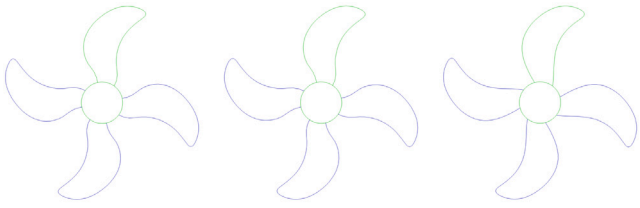

(a) Runs R_{2-OP1}, R_{3-OP1}, R_{4-OP1}

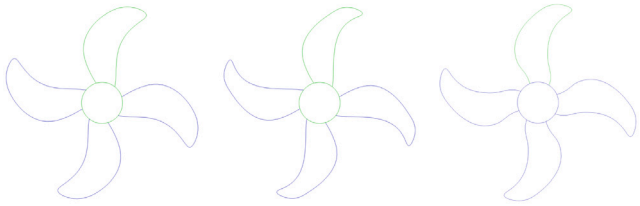

(b) Runs R_{5-OP1}, R_{5b-OP1}, R_{5c-OP1}

Fig. 18. Geometry of the best designs — OP_1.

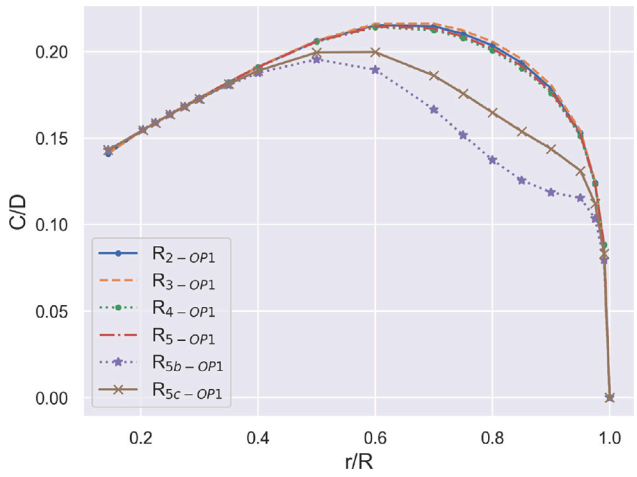

Fig. 19. C/D of the best designs — OP_1.

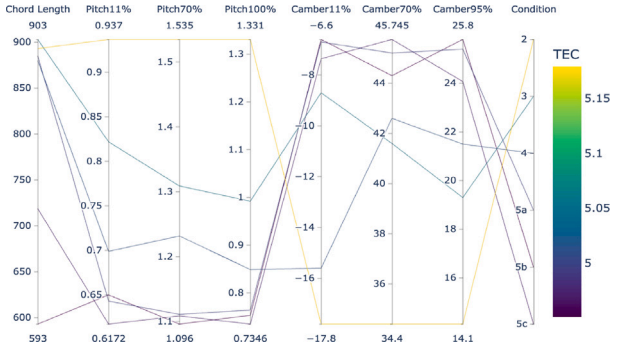

Fig. 20. PCV of the best designs — OP_1.

Finally, we examined how the optimal design of OP_1 performs in OP_2 and the other way around. The optimal design of OP_1, in terms of TEC and feasible geometry, was obtained from run R_{5c-OP1} with a TEC of 4.97 GWh/yr and the optimal design of OP_2 was obtained from run R_{5b-OP2} with TEC equal to 4.66 GWh/yr. If the optimal design of OP_1 would operate under OP_2, then the TEC would be 4.65 GWh/yr, which means that it would give a bit lower energy consumption than the optimal design of OP_2. Moreover, if the optimal design of OP_2 would

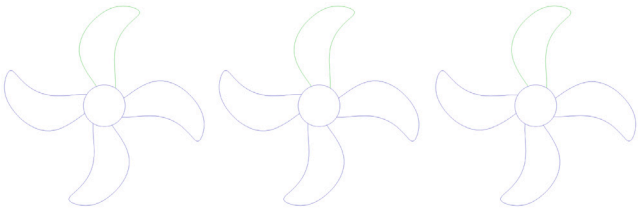

(a) Runs R_{2-OP2}, R_{3-OP2}, R_{4-OP2}

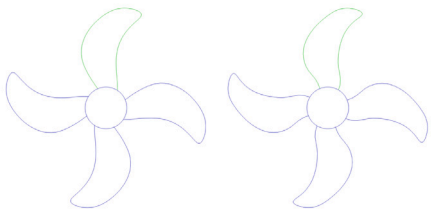

(b) Runs R_{5-OP2}, R_{5b-OP2}

Fig. 21. Geometry of the best designs — OP_2.

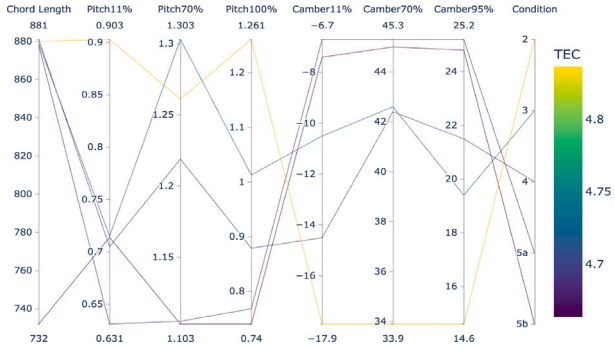

Fig. 22. PCV of the best designs — OP_2.

operate under OP_1, the TEC would be equal to 4.98 GWh/yr, which is a bit above the TEC of the optimal design of OP_1. The differences are very small though and it seems that both designs operate well in both conditions.

6.2.4. Design space

The search of the design space of R_{5b-OP2}, which offered the lowest TEC, is presented in this section. In Fig. 23, a PCV is plotted separately for each design variable and the TEC. The pitch, camber and chord length are presented in the upper, middle and lower plots respectively. The goal of these plots is to better understand which areas of the design space lead to reduced TEC, so that in future studies we adapt the optimisation search towards those areas.

Regarding the pitch, it seems that in order to obtain low TEC, the algorithm led to increased values of pitch at 0.13R and to decreased values at 0.7R. In more detail, values above 0.55 at 0.13R, below 1.12 at 0.7R and between 0.7 and 0.8 at 1.0R, led to lower TEC.

From the camber plots it is shown that low values of TEC are achieved with increased camber at 0.7R and 1.0R, whereas the camber at 0.13R did not affect the results. More specifically, values above 43 at 0.7R and above 25 at 1.0R offered lower TEC.

Finally, regarding the values of the chord length, it seems that low TEC is obtained with low values of chord length, close to the minimum limits. Low TEC was achieved with values lower than 1075 at 0.7R and lower than 800 at 0.9R.

More detailed plots about the design space of all runs for both operational profiles can be found at the Appendix. A PCV of each design variable is presented separately; for the pitch in Figs. 25 and

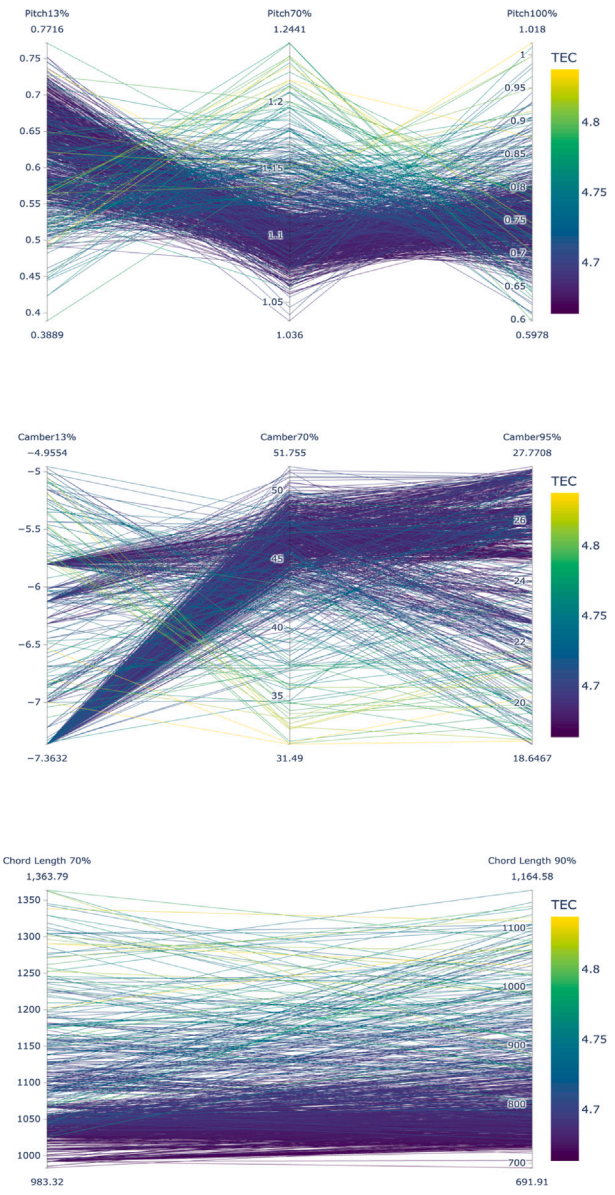

Fig. 23. Design space of run R_{5b-OP2}.

28, for the camber in Figs. 26 and 29 and finally for the chord length in Figs. 27 and 30. In each plot, the design space of the variables is shown for every run, R_{2-OP1}-R_{5c-OP1} for OP_1 and R_{2-OP2}-R_{5b-OP2} for OP_2. The values of the ranges of each run are different, because the starting designs are different and in the runs R_{5b-OP1}, R_{5C-OP1} and R_{5b-OP2}, wider limits have been set. The trend of the values of the design variables for achieving low TEC is similar as for R_{5b-OP2}. In OP_2 though, the separation for the values regarding low or high TEC is more apparent, because longer optimisation runs were performed.

6.2.5. Cavitation evaluation

Due to the wide operation of the vessel and the propeller, it was expected that in this study, suction side cavitation would appear at the more highly loaded conditions and maybe at the middle loaded as well, and pressure side cavitation would appear at the two more lightly loaded conditions. However, cavitation (of any type) did not appear almost at all during the study. Most probably this is due to the fact that the hull has been optimised for wind-propulsion, with sailing 50% of the time, something that resulted in a more homogeneous inflow to the propeller.

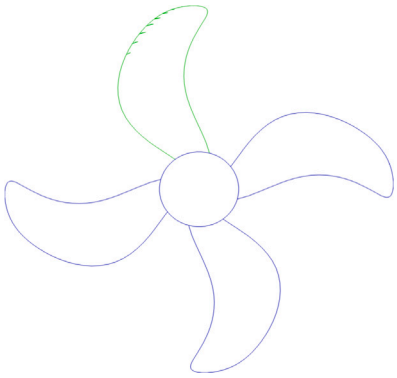

Fig. 24. Cavitation evaluation at optimisation run R_{2-OP2} for analysis condition C_5.

When we performed the optimisation for the OP_2, for the optimisation run R_{2-OP2} (one of the two most lightly loaded conditions), and the cavitation of the propeller was evaluated by the blade designer for all conditions, some suction side cavitation appeared in some designs at the analysis condition C_5. The cavity volume was low and the cavity shape smooth, as shown in Fig. 24, thus designs that had these cavitation characteristics were assessed as accepted. The optimal design of this run though did not have any cavitation.

7. Conclusion

In this study, we presented a methodology for the design and optimisation of propellers for wind-powered ships with the aim to cover the demanding operating needs of wind propulsion. The case study of this paper regards the design of a CPP (controllable-pitch propeller) for the Oceanbird research concept of a wPCC (wind-powered car-carrier). The wPCC is equipped with four identical, rigid wing sails and it does a transatlantic crossing between two fixed destinations operating at constant speed. It is primarily designed for sailing and the propeller operates in a wide range of loading conditions, from very lightly loaded, up to highly loaded conditions, when the engine is needed for extra powering. Several conditions of the operational profile have been included in the design and optimisation process, while the objective has been to obtain a design that represents a feasible propeller geometry with minimised TEC (total energy consumption).

For the part of the journey that the propeller does not operate, due to suitable weather conditions for wind-powering, the three functions of windmilling, feathering and harvesting were investigated, in order to understand which function would be more advantageous. According to the results, the feathering function of the CPP propeller offered the lowest drag over the ship resistance, when compared to a windmilling FPP or CPP. Regarding the harvesting operation, it is very important to consider the shaft losses early and try to reduce them as much as possible.

The lowest TEC was achieved for both operational profiles with the optimisation runs that had as a starting point the most highly loaded condition. It seems that although the least time was spent in that condition, the delivered power was very high and this resulted in high energy consumption. For this study and the specific two operational profiles, it was more advantageous to optimise the blade design based on highly loaded conditions, since the effect of the more lightly loaded conditions was not as important for the calculation of TEC. To be more precise, when we had as a starting point of the optimisation the baseline of a lightly loaded condition, the efficiency in the highly loaded conditions was not that high, something that increased the delivered power of the more highly loaded conditions and this had a negative impact on the TEC.

The investigation of the design space showed that lower TEC was achieved with decreased pitch values at 0.7R, high camber values at

0.7R and 0.95R and with minimum chord length. The wider limits in the design variables offered lower TEC, but the variable curves should be controlled so that we do not end up with infeasible geometries.

Interesting results were obtained for the cavitation, since almost no cavitation appeared in all conditions. As it was mentioned earlier, although the hull was designed for sailing in lightly loaded conditions, some cavitation was still expected to appear. Therefore, it would be interesting to compare the results with those of other future studies in wind propulsion and with hydrodynamic analysis tools of higher fidelity.

We believe that the optimisation approach we propose is straightforward and fulfils the goals of propeller design in wind propulsion. The objective of TEC guides the optimisation towards areas of the design space with improved performance over a wide range of operating conditions. It should be mentioned though that the larger the operational profile, the more time-consuming the optimisation is, because the hydrodynamic analysis is performed for both design and analysis conditions of each one design out of the thousands ones.

The route simulations are an important input in our design process for defining the operational profile of the propeller. Further investigation is therefore needed for the data used in the simulations, in order to be sure that we design and optimise for the correct operation.

Another point is that it would be beneficial to have the detailed engine information early in the design process, in order to compute the TFC (total fuel consumption) and investigate the emission reduction based on more accurate data. Generally the engine should operate in its optimum point where the SFC (specific fuel consumption) is at its lowest. In cases with so many operating conditions and with large load variation, the SFC will have a wide variation as well. Therefore for an engine with such large powering, the optimum point will be far from the lightly loaded conditions. This means that except the propeller load, also the potential high SFC in those conditions may lead to a feathered/windmilling propeller.

CRediT authorship contribution statement

Ioli Gypa: Conceptualization, Methodology, Visualization, Writing – original draft. **Marcus Jansson:** Conceptualization, Methodology, Software, Writing – review & editing. **Robert Gustafsson:** Conceptualization, Methodology, Writing – review & editing. **Sofia Werner:** Conceptualization, Methodology, Writing – review & editing. **Rickard Bensow:** Conceptualization, Methodology, Writing – review & editing, Supervision.

Declaration of competing interest

The authors declare that they have no known competing financial interests or personal relationships that could have appeared to influence the work reported in this paper.

Data availability

No data was used for the research described in the article.

Acknowledgements

Funding for this study was provided by Chalmers University of Technology Foundation, Sweden for the strategic research project Hydro- and aerodynamics; by the Swedish Transportation Agency via Lighthouse through the SailProp project; and by Kongsberg Maritime Sweden AB through the University Technology Centre in Computational Hydrodynamics hosted at the Department of Mechanics and Maritime Sciences at Chalmers.

Appendix

See Figs. 25–30.

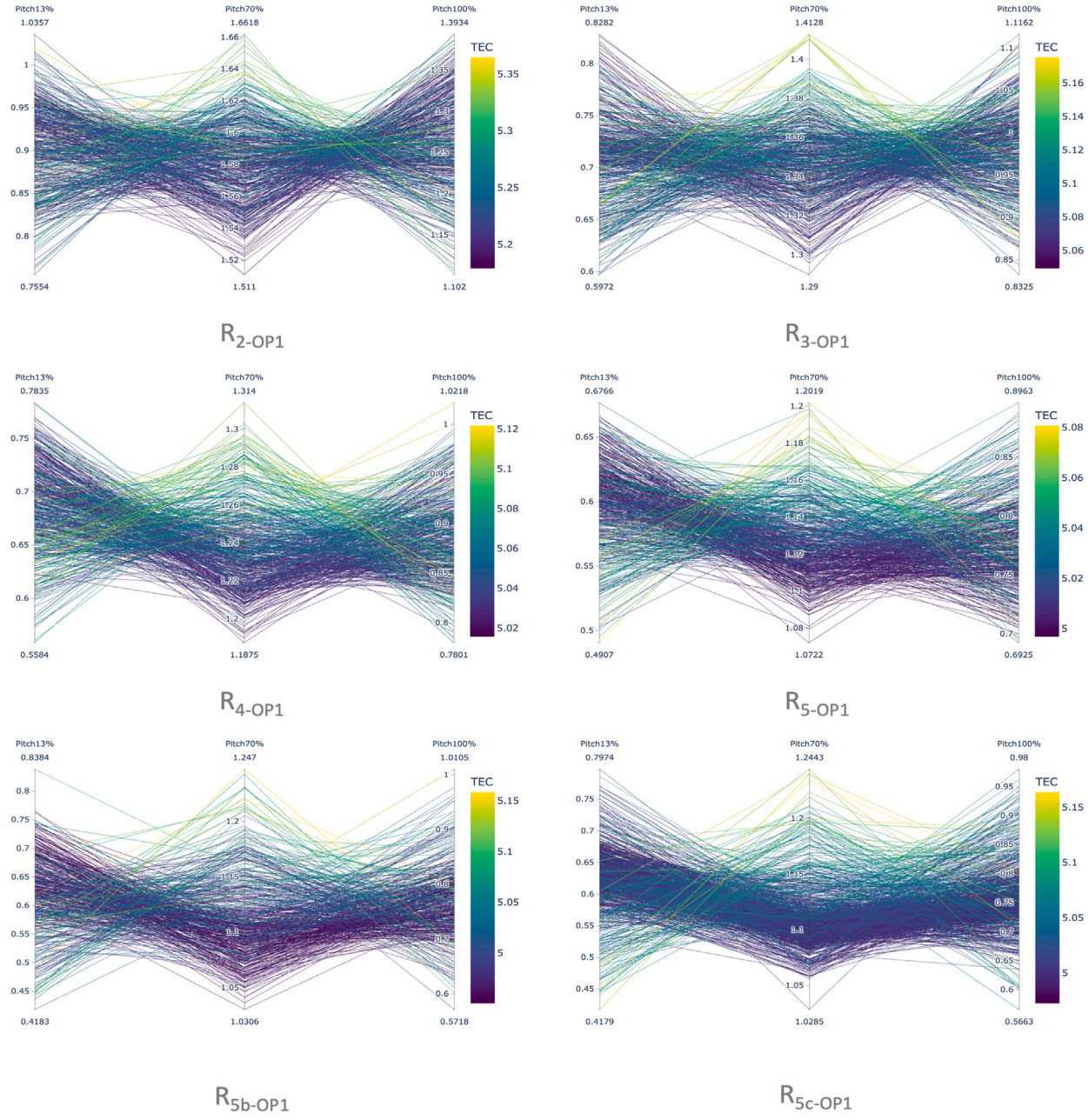

Fig. 25. Design space – OP1 – Pitch.

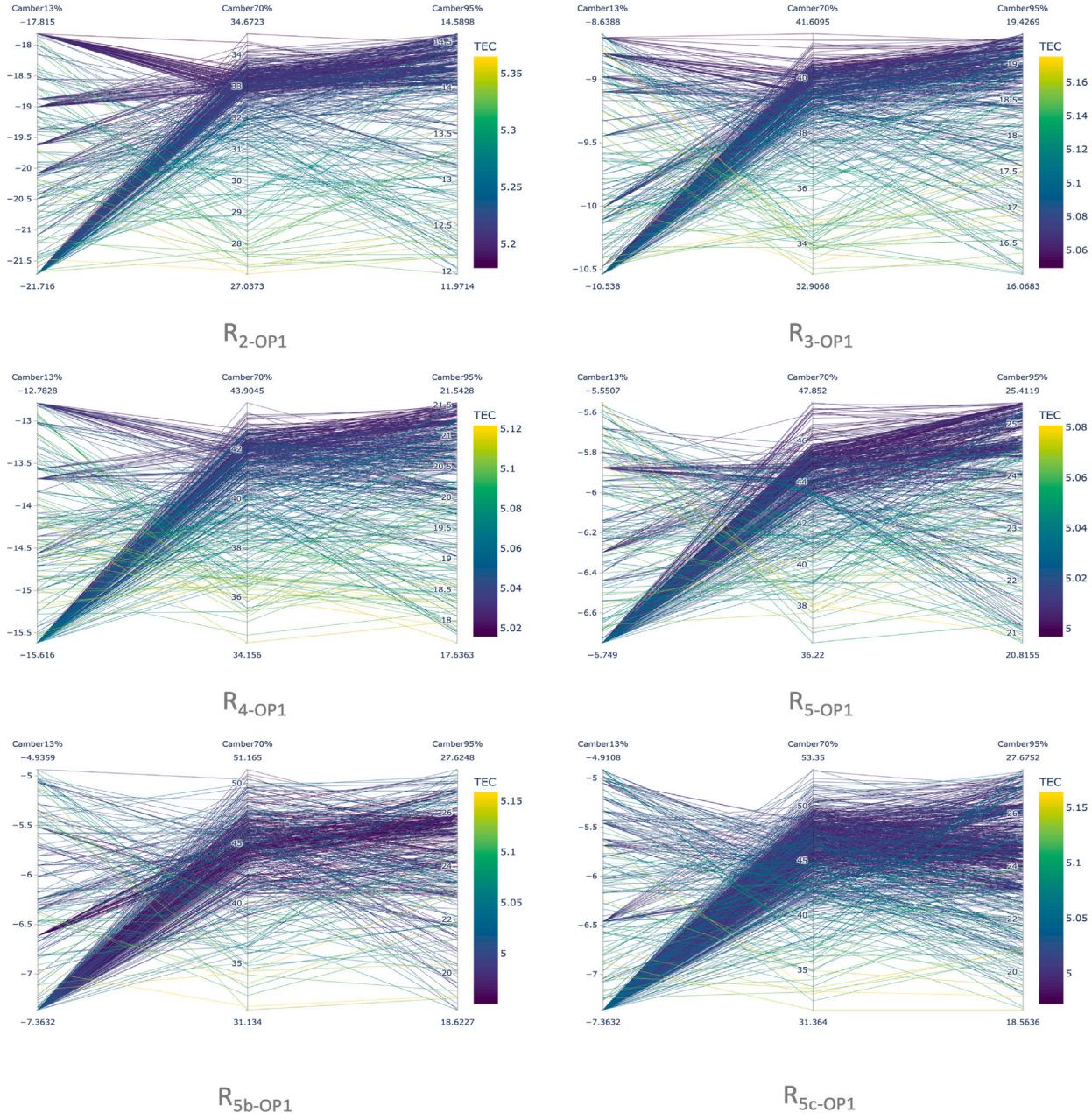

Fig. 26. Design space – OP1 – Camber.

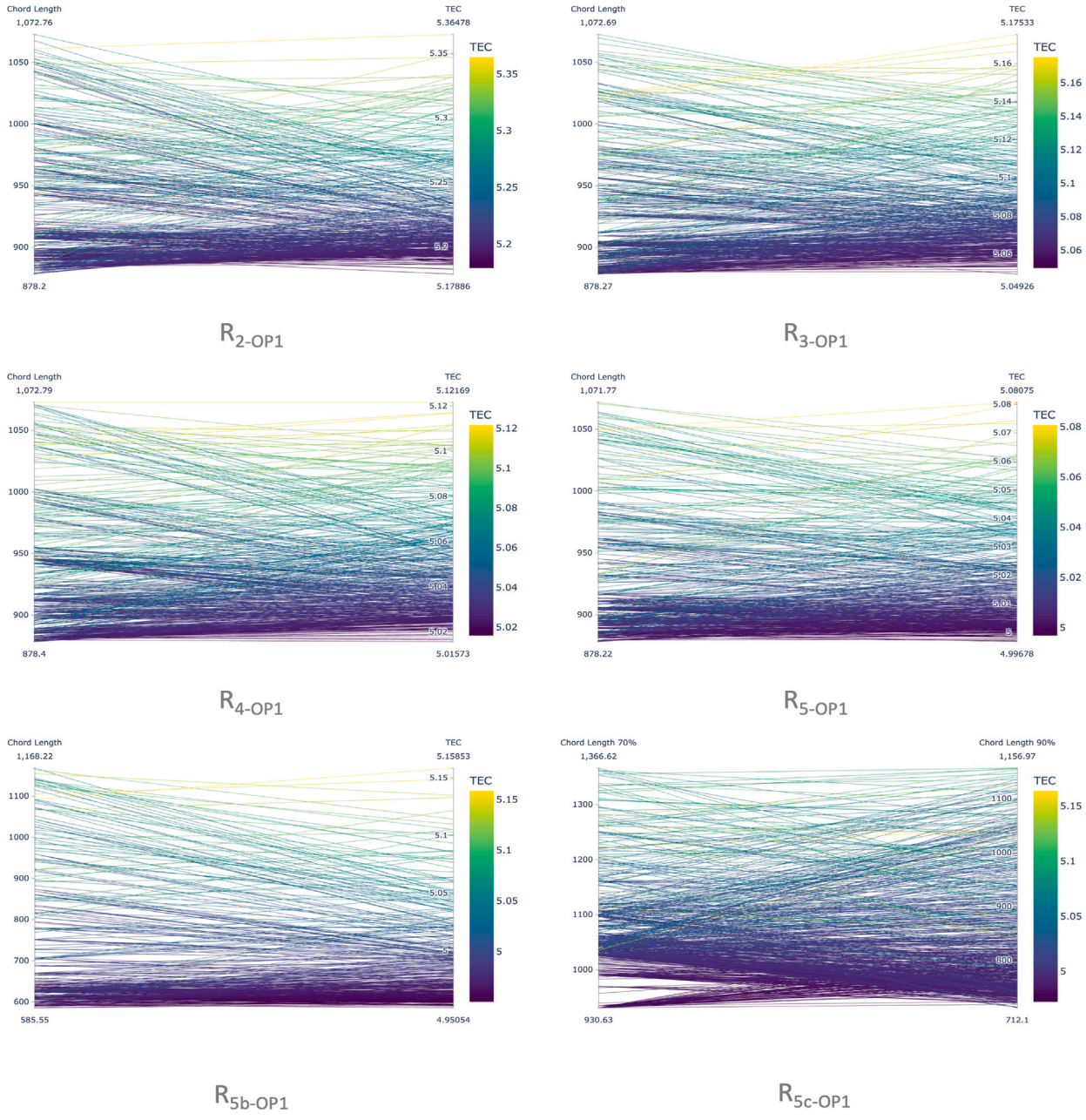

Fig. 27. Design space – OP1 – Chord length.

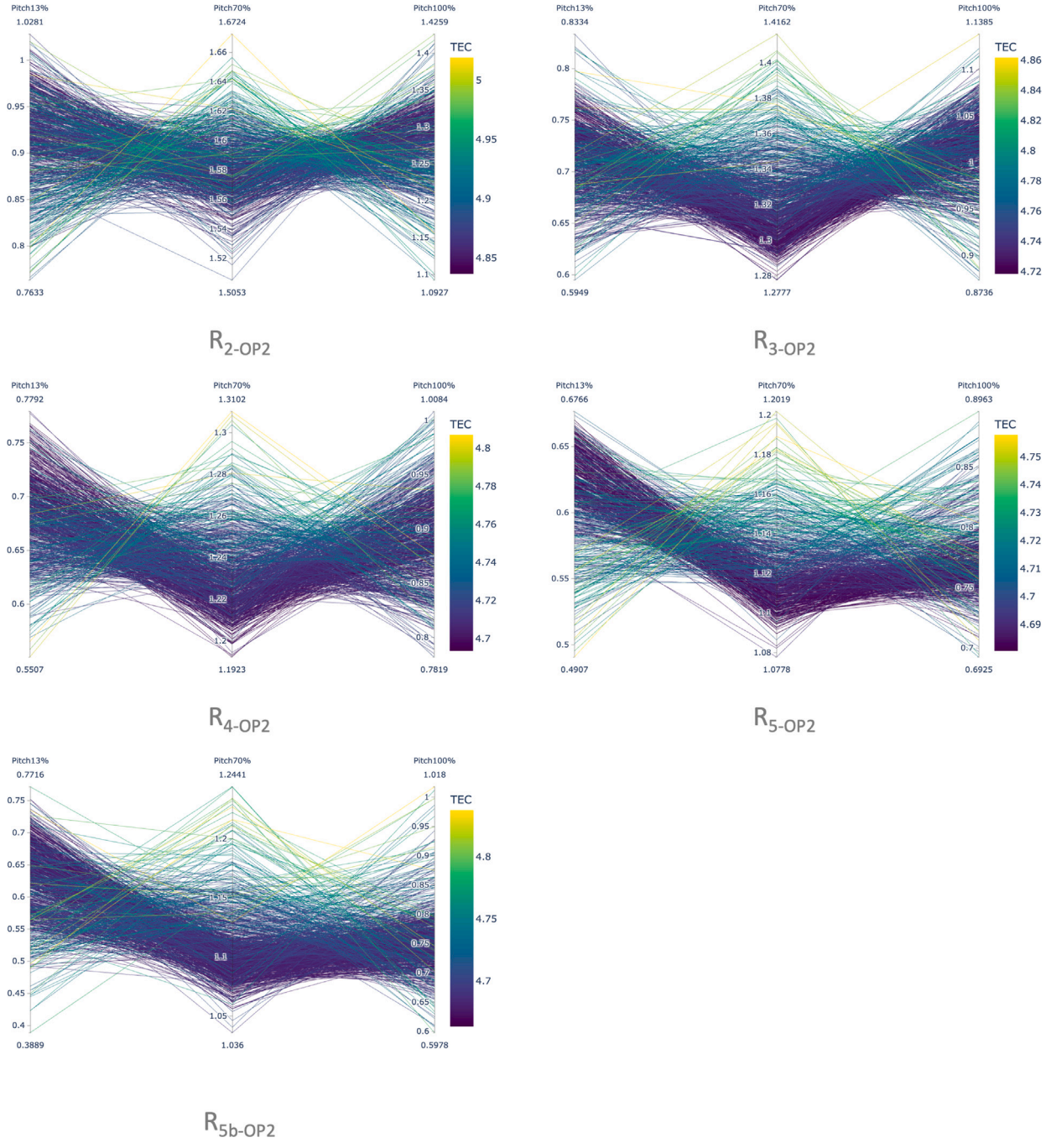

Fig. 28. Design space – OP2 – Pitch.

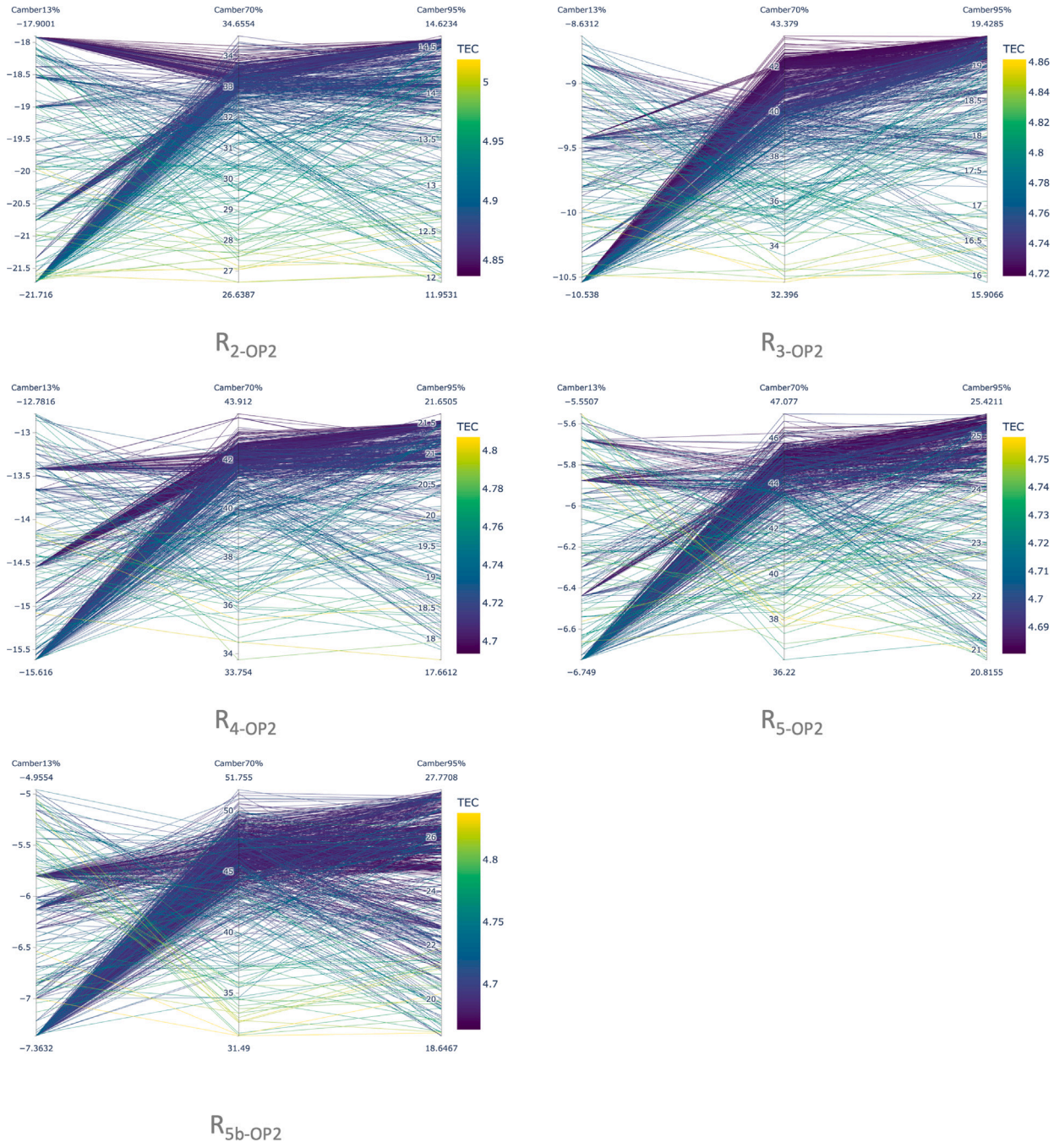

Fig. 29. Design space – OP2 – Camber.

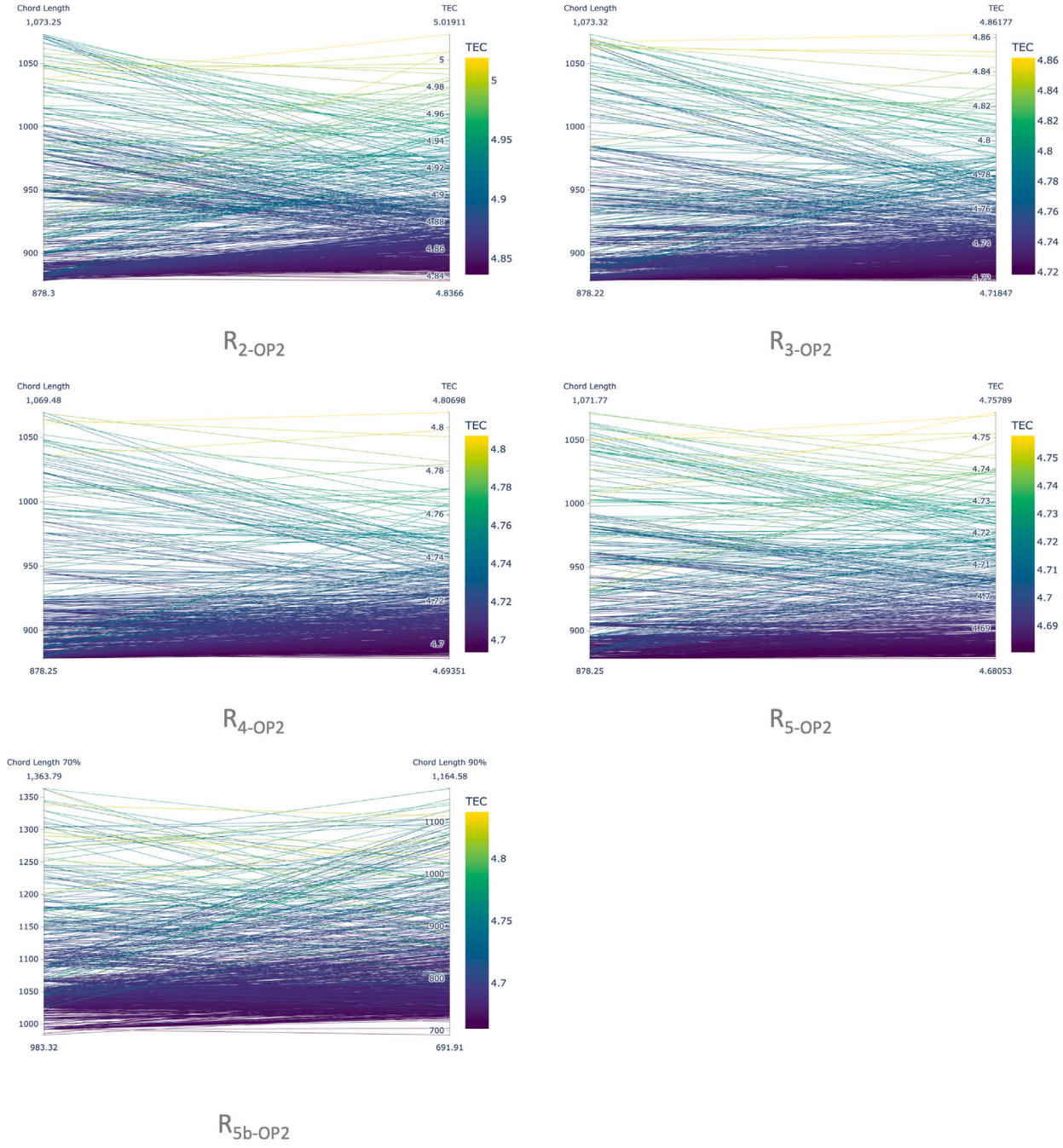

Fig. 30. Design space – OP2 – Chord length.

References

Andersson, J., Gustafsson, R., Eslamdoost, A., Bensow, R.E., 2021. On the selection of optimal propeller diameter for a 120-m cargo vessel. J. Ship Res. 65 (02), 153–166.

Balcombe, P., Brierley, J., Lewis, C., Skatvedt, L., Speirs, J., Hawkes, A., Staffell, I., 2019. How to decarbonise international shipping: Options for fuels, technologies and policies. Energy Convers. Manage. 182, 72–88.

Carlton, J., 2018. Marine Propellers and Propulsion. Butterworth-Heinemann.

Carlton, J., Aldwinkle, J., Anderson, J., et al., 2013. Future ship powering options: exploring alternative methods of ship propulsion. Lond. R. Acad. Eng..

Chou, T., Kosmas, V., Acciaro, M., Renken, K., 2021. A comeback of wind power in shipping: An economic and operational review on the wind-assisted ship propulsion technology. Sustainability 13 (4), URL https://www.mdpi.com/2071-1050/13/4/1880.

COP26 Declaration, 2021. Clydebank declaration for green shipping corridors. https://ukcop26.org/cop-26-clydebank-declaration-for-green-shipping-corridors/.

Copernicus Climate Data Store, 2022a. Copernicus climate data store. https://cds.climate.copernicus.eu/, (Accessed 10 July 2022).

Dang, J., Van Den Boom, H., Ligtelijn, J.T., 2013. The Wageningen C-and D-series propellers. In: 12th International Conference on Fast Sea Transportation FAST. Citeseer.

Gypa, I., Jansson, M., Gustafsson, R., Werner, S., Bensow, R., 2022. Propeller design procedure for a wind-assisted KVLCC2. In: 15^{Th} International Symposium on Practical Design of Ships and Other Floating Structures. Dubrovnik, Croatia.

Gypa, I., Jansson, M., Wolff, K., Bensow, R., 2021. Propeller optimization by interactive genetic algorithms and machine learning. Ship Technol. Res. 1–16. http://dx.doi.org/10.1080/09377255.2021.1973264.

He, L., Chang, S., Kinnas, S., 2010. MPUF-3A Version 3.0. Technical Report, University of Texas.

IEA, 2021a. Greenhouse gas emissions from energy: Overview.

IEA, 2021b. Tracking transport 2021.

IMO, 2020. Fourth IMO GHG study 2020.

IMO Resolution MEPC.304(72), 2018. Initial IMO strategy on reduction of GHG emissions from ships.

Kerwin, J., Kinnas, S., Wilson, M.B., 1986. Experimental and analytical techniques for the study of unsteady propeller sheet cavitation. In: Symposium on Naval Hydrodynamics, 16th. Berkeley, California.

Kinnas, S., Lee, H., Young, Y.L., 2003. Modeling of unsteady sheet cavitation on marine propeller blades. Int. J. Rotating Mach. 9, http://dx.doi.org/10.1155/S1023621X03000241.

Kongsberg hydrodynamic design team, 2022. Private communication.

Korberg, A.D., Brynolf, S., Grahn, M., Skov, I.R., 2021. Techno-economic assessment of advanced fuels and propulsion systems in future fossil-free ships. Renew. Sustain. Energy Rev. 142, 110861. http://dx.doi.org/10.1016/j.rser.2021.110861, URL https://www.sciencedirect.com/science/article/pii/S1364032121001556.

Lee, C.S., 1979. Prediction of steady and unsteady performance of marine propellers with or without cavitation by numerical lifting-surface theory. (Ph.D. thesis). Massachusetts Institute of Technology.

Leloup, R., Roncin, K., Behrel, M., Bles, G., Leroux, J.B., Jochum, C., Parlier, Y., 2016. A continuous and analytical modeling for kites as auxiliary propulsion devoted to merchant ships, including fuel saving estimation. Renew. Energy 86, 483–496. http://dx.doi.org/10.1016/j.renene.2015.08.036, URL https://www.sciencedirect.com/science/article/pii/S0960148115302366.

Leloup, R., Roncin, K., Bles, G., Leroux, J.B., Jochum, C., Parlier, Y., 2014. Kite and classical rig sailing performance comparison on a one design keel boat. Ocean Eng. 90, 39–48.

Lu, R., Ringsberg, J.W., 2020. Ship energy performance study of three wind-assisted ship propulsion technologies including a parametric study of the flettner rotor technology. Ships Offshore Struct. 15 (3), 249–258.

Malmek, K., Dhomé, U., Larsson, L., Werner, S., Ringsberg, J., Finnsgard, C., 2020. Comparison of two rapid numerical methods for predicting the performance of multiple rigid wing-sails. In: the 5th International Conference on Innovation in High Performance Sailing Yachts and Sail-Assisted Ship Propulsion (INNOV'sAIL 2020). Gothenburg, Sweden, pp. 49–58.

Molland, A.F., Hawksley, G.J., 1985. An investigation of propeller performance and machinery applications in wind assisted ships. J. Wind Eng. Ind. Aerodyn. 20, 143–168.

Olsson, F., Giovannetti, L., Werner, S., Finnsgård, C., 2020. A performance depowering investigation for wind powered cargo ships along a route. J. Sailing Technol. 5 (01), 47–60.

Seddiek, I.S., Ammar, N.R., 2021. Harnessing wind energy on merchant ships: case study Flettner rotors onboard bulk carriers. Environ. Sci. Pollut. Res. 28 (25), 32695–32707.

Talluri, L., Nalianda, D.K., Giuliani, E., 2018. Techno economic and environmental assessment of Flettner rotors for marine propulsion. Ocean Eng. 154, 1–15.

The Oceanbird Concept, https://www.theoceanbird.com/the-oceanbird-concept/, (Accessed 10 July 2022).

Tillig, F., Ringsberg, J.W., 2020. Design, operation and analysis of wind-assisted cargo ships. Ocean Eng. 211, 107603. http://dx.doi.org/10.1016/j.oceaneng.2020.107603, URL https://www.sciencedirect.com/science/article/pii/S0029801820306077.

Traut, M., Gilbert, P., Walsh, C., Bows, A., Filippone, A., Stansby, P., Wood, R., 2014. Propulsive power contribution of a kite and a Flettner rotor on selected shipping routes. Appl. Energy 113, 362–372.

UNFCCC, 2015. 21st Session of the Conference of the Parties and 11th Session of the Conference of the Parties serving as the meeting of the Parties to the Kyoto Protocol- UNFCCC COP 21/ CMP 11.

Vesting, F., 2015. Marine Propeller Optimisation - Strategy and Algorithm Development (Ph.D. thesis). Chalmers University of Technology.

Viola, I.M., Sacher, M., Xu, J., Wang, F., 2015. A numerical method for the design of ships with wind-assisted propulsion. Ocean Eng. 105, 33–42. http://dx.doi.org/10.1016/j.oceaneng.2015.06.009, URL https://www.sciencedirect.com/science/article/pii/S0029801815002528.

Werner, S., 2021. SAILPROP: Operational profile for a Wind Powered Vehicle Carrier. Technical Report RE40209596-02-00-A, SSPA Sweden AB.